Microsecond Photoluminescence and Photoreactivity of a Metal-Centered Excited State in a Hexacarbene – Co(III) Complex

Simon Kaufhold, Nils W. Rosemann, Pavel Chábera, Linnea Lindh, Iria Bolano Losada, Jens Uhlig, Torbjörn Pascher, Daniel Strand, Kenneth Wärnmark, Arkady Yartsev, and Petter Persson

Supporting Information

Synthesis and standard characterisation of $[Co(PhB(MeIm)_3)_2]PF_6$

All reactions were carried out using standard Schlenk techniques. Size-exclusion chromatography was performed on BioBeads S-X1 gel (Bio-Rad, column size d = 40 × h = 1200 mm). ^1H and ^{13}C NMR spectra were recorded on a Bruker Avance II 400 MHz NMR spectrometer. Chemical shifts (δ) are reported to the shift-scale calibrated with the residual NMR solvent; CD_3CN (1.94 ppm for ^1H NMR spectra and 1.32 and 118.26 ppm for ^{13}C NMR spectra). Electrospray ionization high-resolution mass spectrometry (ESI–HRMS) was recorded on a Waters XEVO-G2 Q-ToF mass spectrometer. Elemental analysis was performed by Mikroanalytisches Laboratorium KOLBE (Mülheim an der Ruhr, Germany). KO*t*Bu (1 M solution in THF), NH_4PF_6, KPF_6 and Na_2SO_4 were purchased from Sigma-Aldrich. Anhydrous cobalt(II) chloride was purchased from ACROS Organics. CH_2Cl_2, *N*,*N*-dimethylformamide (DMF) Et_2O, MeCN, tetrahydrofuran (THF) and toluene were purchased from VWR, Fisher Scientific or Sigma-Aldrich. THF was dried over Na/benzophenone and was subsequently distilled under an atmosphere of nitrogen gas prior to use. Anhydrous MeCN and DMF were obtained from a PureSolv PSM-768 and MBraun SPS-800 system, respectively. Tris(3-methylimidazolium-1-yl)(phenyl)borate bis(hexafluorophosphate) $(PhB(MeIm)_3)(PF_6)_2$ was synthesized using literature methods.[1,2]

$[Co(PhB(MeIm)_3)_2]PF_6$ was synthesised in analogy to previously reported procedures for Fe-NHC complexes.[2,3]

Procedure A:

An oven-dried 100 mL Schlenk tube with stirring bar was charged with $(PhB(MeIm)_3)(PF_6)_2$ (624 mg, 1.00 mmol, 1 eq.) and $CoCl_2$ (77 mg, 0.60 mmol, 0.6 eq.) under a flow of N_2. Subsequently, the solids were heated to 80 °C under house vacuum overnight. The Schlenk tube was purged with N_2 and allowed to cool to room temperature. Dry THF (45 mL) was added and the resulting light blue suspension was cooled to -78 °C in an acetone/dry ice bath. KO*t*Bu (3.5 mL, 1 M in THF, 3.5 eq) was added dropwise over 10 min and the resulting dark blueish reaction mixture was allowed to warm to room temperature under exclusion of light and stirred overnight. After opening the Schlenk tube to air a colour change to dark brown was observed and the solvent was removed under reduced pressure. The residue was taken up in CH_2Cl_2 (150 mL) and filtered through a plug of celite before washing with water (3 x 150 mL). The organic phase was separated and dried over Na_2SO_4, filtered and evaporated to dryness under reduced pressure and further purified as described below.

Procedure B:

An oven-dried 100 mL Schlenk tube with stirring bar was charged with $(PhB(MeIm)_3)(PF_6)_2$ (624 mg, 1.00 mmol, 1 eq.) and $CoCl_2$ (77 mg, 0.60 mmol, 0.6 eq.) under a flow of N_2. Subsequently, the solids were heated to 80 °C under house vacuum overnight. The Schlenk tube was purged with N_2 and allowed to cool to room temperature. Dry DMF (7 mL) was added yielding an intensely blue coloured solution. KO*t*Bu (3.5 mL, 1 M in THF, 3.5 eq.) was added in one portion and the reaction mixture was stirred for 10 min before opening the Schlenk tube to air. To the resulting dark brown mixture, a solution of KPF_6 (ca 1.8 g, 10 eq.) in water (100 mL) was added, leading to a greenish precipitate. The precipitate was filtered off over a sintered funnel (P4) and washed with water (2 x 10 mL). The residue was taken up in CH_2Cl_2 and washed with water (3 x 100 mL). The organic phase was separated and dried over Na_2SO_4 before filtration and removal of solvent under reduced pressure.

Common workup procedure:

The residue was taken up in a minimum amount of MeCN (4-6 mL), filtered through a syringe filter (0.2 µm, PTFE, *d* = 1 cm) and reprecipitated by addition of Et_2O (100-150 mL). This procedure was repeated once or twice until the filtrate was almost colourless. The so obtained beige powder was subjected to size-exclusion column chromatography (MeCN/toluene = 1:1). Usually 2-3 bands appeared with the product eluting closely after the initial brown and yellowish-brown bands and, in case of procedure A, followed by a yellowish band. The solvent was removed, the almost colourless residue taken up in a minimum amount of MeCN, syringe filtered (0.2 µm, PTFE, *d* = 1 cm) and precipitated by addition of Et_2O or toluene or recrystallised by slow evaporation of a MeCN/toluene (1:2) mixture. The product was received as a white powder or colourless crystals in 5% yield (24 mg).

Note: As the product has no apparent colour, it is advisable to collect all fractions of the size-exclusion column and check for the presence of product by evaporation (and NMR analysis). Addition of a few drops of HCl during the first washing with water in the workup can help to avoid contamination the size-exclusion column later.

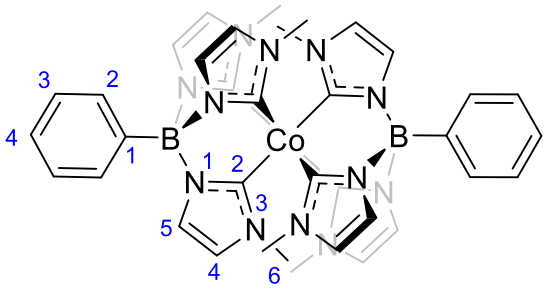

^{1}H-NMR (400 MHz; CD_3CN): δ 8.12 (dd, *J* = 8.2, 1.4 Hz, 4H, Ph-2), 7.63 (tt, *J* = 7.2, 1.6 Hz, 4H, Ph-3), 7.59-7.54 (m, 2H, Ph-4), 7.18 (d, *J* = 1.8 Hz, 6H, Im-5), 6.82 (d, *J* = 1.8 Hz, 6H, Im-4), 2.16 (s, 18H, Im-6).

^{13}C-NMR (101 MHz; CD_3CN): δ 135.4 (Ph-2), 129.13 (Ph-3), 128.96 (Ph-4), 123.5 (Im-5), 122.8 (Im-4), 34.4 (Im-6).

ESI-HRMS (MeCN/CH_2Cl_2/MeOH): *m/z* calculated for $[M\text{-}PF_6]^+$ = $C_{36}H_{40}B_2CoN_{12}^+$ = 719.3090, found 719.3095 (the signal with the lowest *m/z* was chosen from the isotopic pattern in order to be able to compare exact masses of a known combination of isotopes).

Elemental Analysis: % calculated / % found for $C_{36}H_{40}B_2CoF_6N_{12}P$: C (49.91 / 49.86), H (4.65 / 4.69), N (19.40 / 19.42).

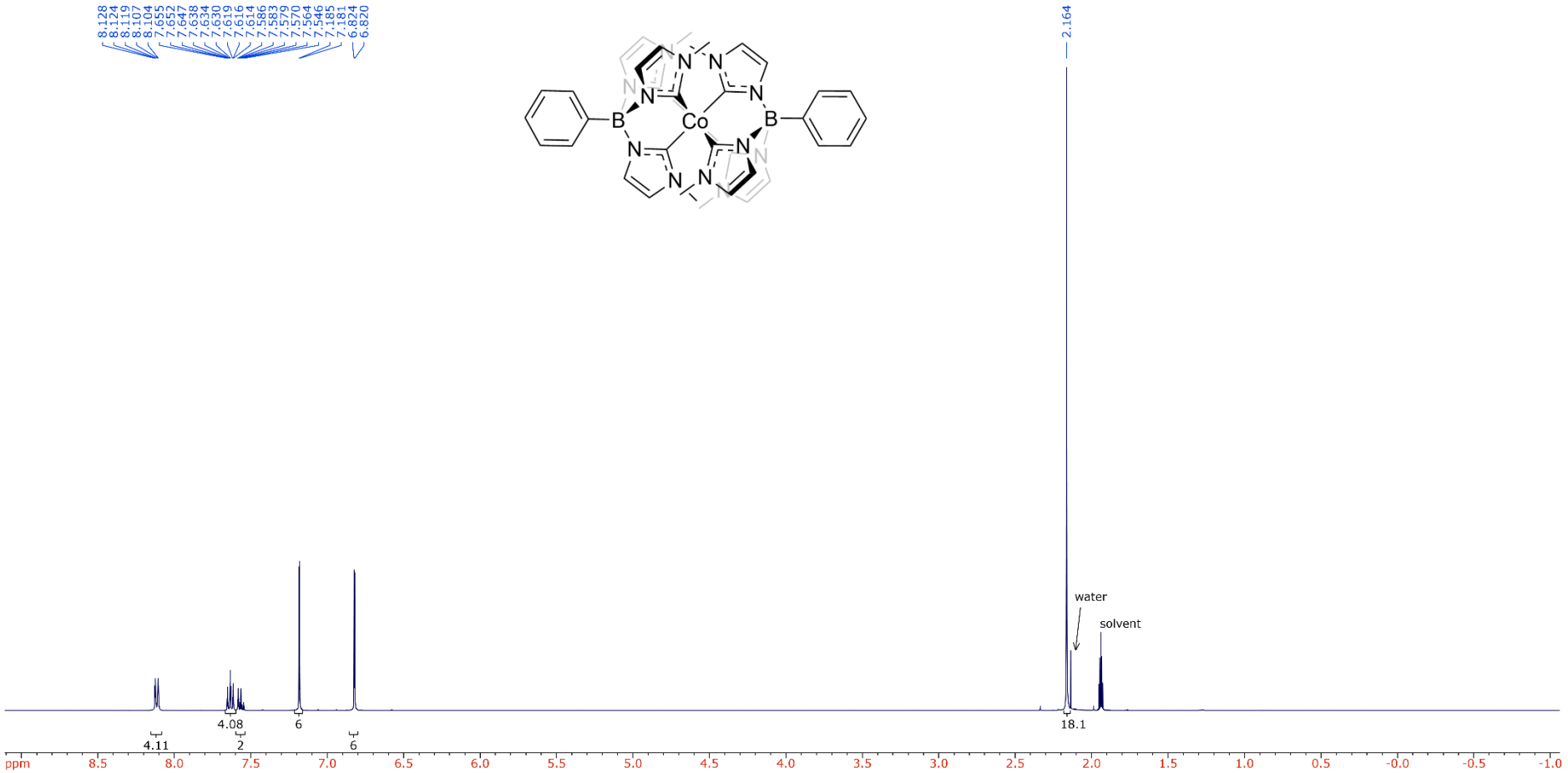

Figure S1: ^{1}H-NMR of $[Co(PhB(MeIm)_3)_2]PF_6$ in MeCN-d3.

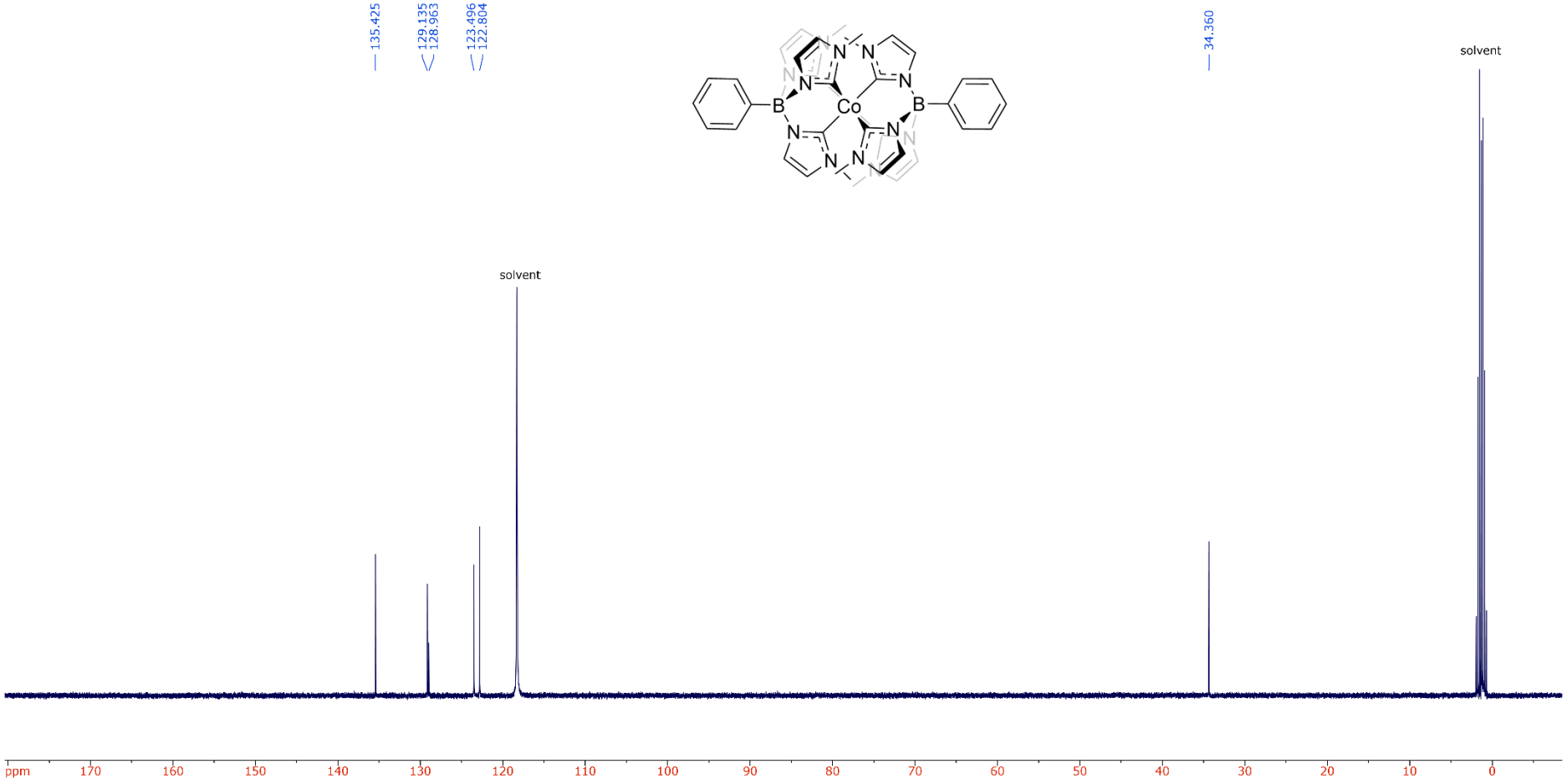

Figure S2: ^{13}C-NMR of $[Co(PhB(MeIm)_3)_2]PF_6$ in MeCN-d3

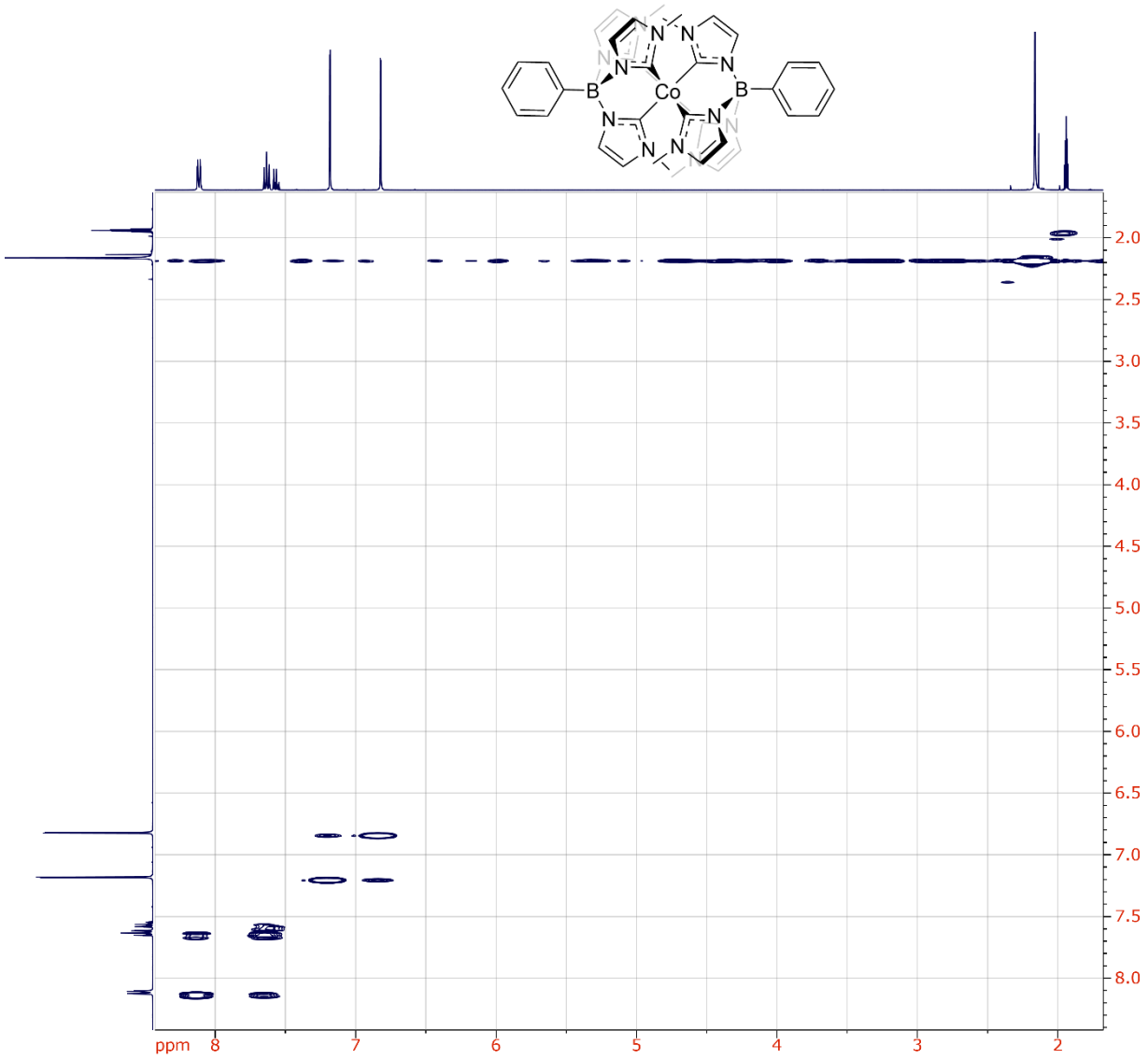

Figure S3: HH-COSY NMR of $[Co(PhB(MeIm)_3)_2]PF_6$ in MeCN-d3.

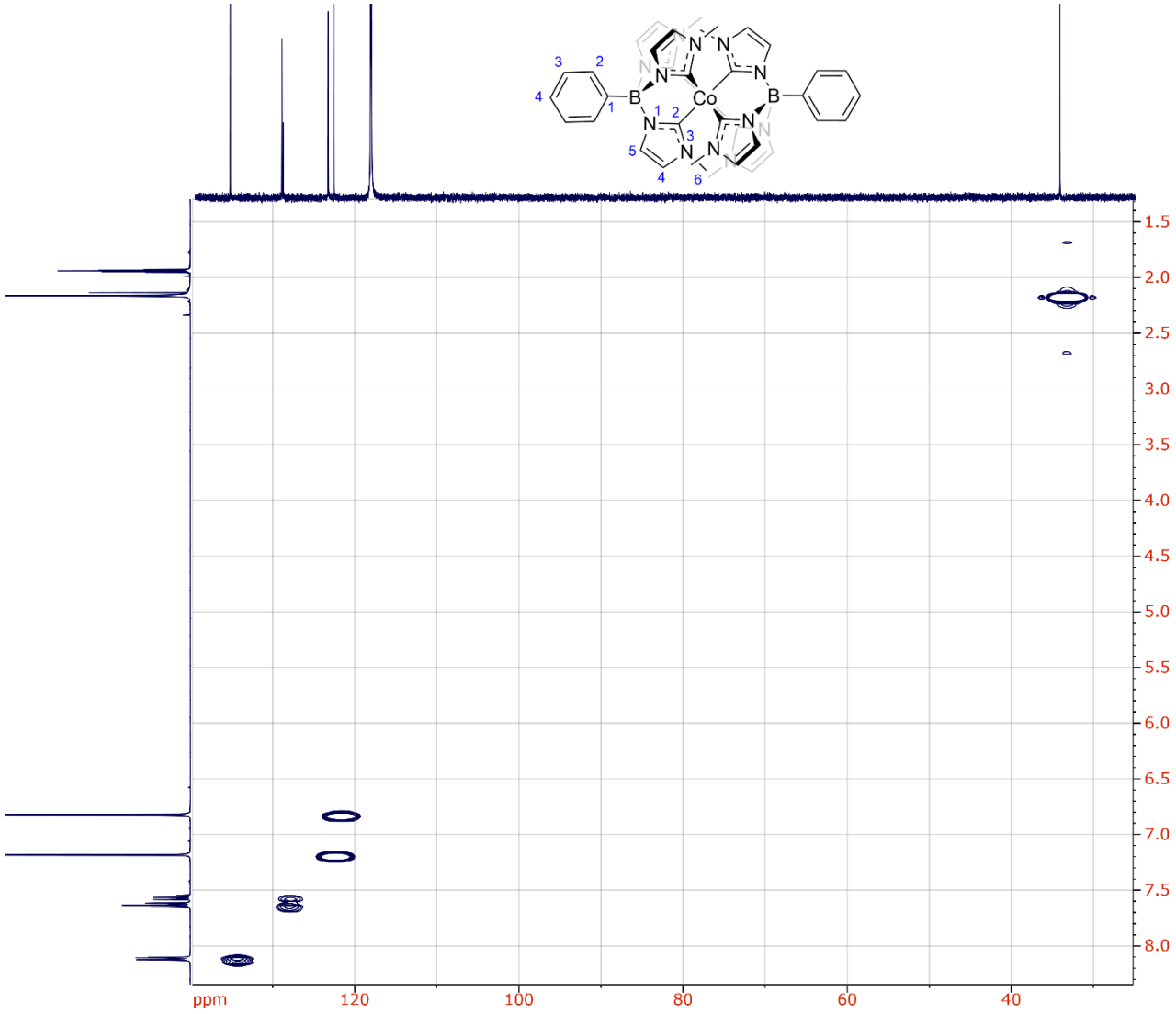

Figure S4: HMQC NMR of $[Co(PhB(MeIm)_3)_2]PF_6$ in MeCN-d3.

Steady state optical spectroscopy

Steady-state absorption measurements were performed using a Perkin Elmer Lambda 1050 UV/Vis/NIR instrument unless stated otherwise. To ensure transparency in the UV range only quartz glass cuvettes (Hellma QS) were used.

Steady state emission measurements were performed on a Horiba Fluorolog-3 fluorimeter. For all measurements Front-Face detection geometry was chosen.

Molar absorption coefficients of $[Co(PhB(MeIm)_3)_2]PF_6$ and the ligand $[PhB(MeImH)_3]^{2+}$ in MeCN is summarized in Table S1. The molar absorption coefficient was estimated from absorption measurements of a carefully prepared dilution series with known concentrations below 1 mM. The quartz glass cuvette was rinsed and dried between each measurement. After background correction, a linear fit of absorption versus concentration was performed at each wavelength to calculate the molar extinction coefficient according to the Beer-Lambert law.

To resolve the weak absorption features observed at wavelength longer than 400 nm an additional measurement at very high sample concentration of 5.6 mM was performed.

Table S1: Molar absorption coefficients of $[Co(PhB(MeIm)_3)_2]^+$ and $(PhB(MeIm)_3)^{2-}$ at selected wavelengths.

Wavelength (nm)	ε $[Co(PhB(MeIm)_3)_2]^+$ [L/mol*cm]	ε $[PhB(MeIm)_3]^{2+}$ [L/mol*cm]
212	63 800	21 300
250	18 900	100
260	11 700	200
310	400	40
400	2.2	---
500	0.4	---

Stability tests

To examine the stability of the $[Co(PhB(MeIm)_3)_2]^+$ complex in solution we performed long-term steady-state absorption measurements. The sample solution was prepared using deaerated acetonitrile that has been bubbled with argon prior to use. To avoid uptake of oxygen sample preparation was performed under nitrogen gas flow. The sample was then stored in fused quartz (Hellma QS) 1 mm optical path-length cuvette sealed with a stopper and additional parafilm. Concentrations of the solution was at 725 ± 20 µM based on the absorbance measured directly after sample preparation.

Over the course of 70 days we performed steady-state absorption measurements on irregular intervals. Between the measurements the sample was stored in the dark, inside the lab bench drawer. The absorption spectra of the measurement series are shown in Figure S5. Even after 70 days no significant changes of the spectrum are observed.

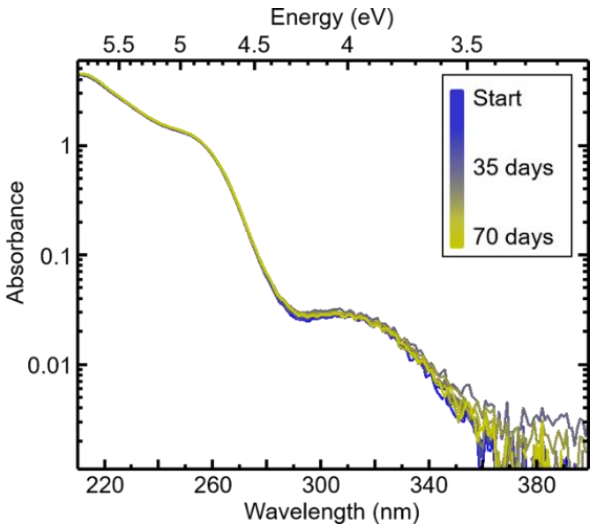

Figure S5: Absorbance spectra of $[Co(PhB(MeIm)_3)_2]^+$ at 0.725 mM concentration in acetonitrile plotted on semi-logarithmic scale. The spectra were measured in irregular intervals over the course of 70 days. Sample was prepared in deaerated solvent in 1 mm optical path length quartz cuvette.

To test the photostability, the complex was dissolved in filtered and dried acetonitrile and sealed airtight in a cuvette. The cuvette was exposed to light of a fluorescence bulb primarily emitting at 254 nm with a small (<5%) 365 nm emission contribution and negligible environmental light contributions. The sample was exposed to UV light for >80 hours. To avoid heating of the sample, the cuvette was kept under constant airflow in a temperature-stabilized laboratory. In irregular intervals, the steady-state absorption spectrum was measured using an Agilent 8453 UV-VIS spectrometer and background corrected as shown in Figure S6 left. The exposure time was converted into turn-over-numbers (TON, number of photons absorbed per molecule) using the illumination intensity and sample concentration. As seen in Figure S6 (right) which shows fractional changes at given wavelengths plotted versus TON the sample is stable for at least 200 turnovers.

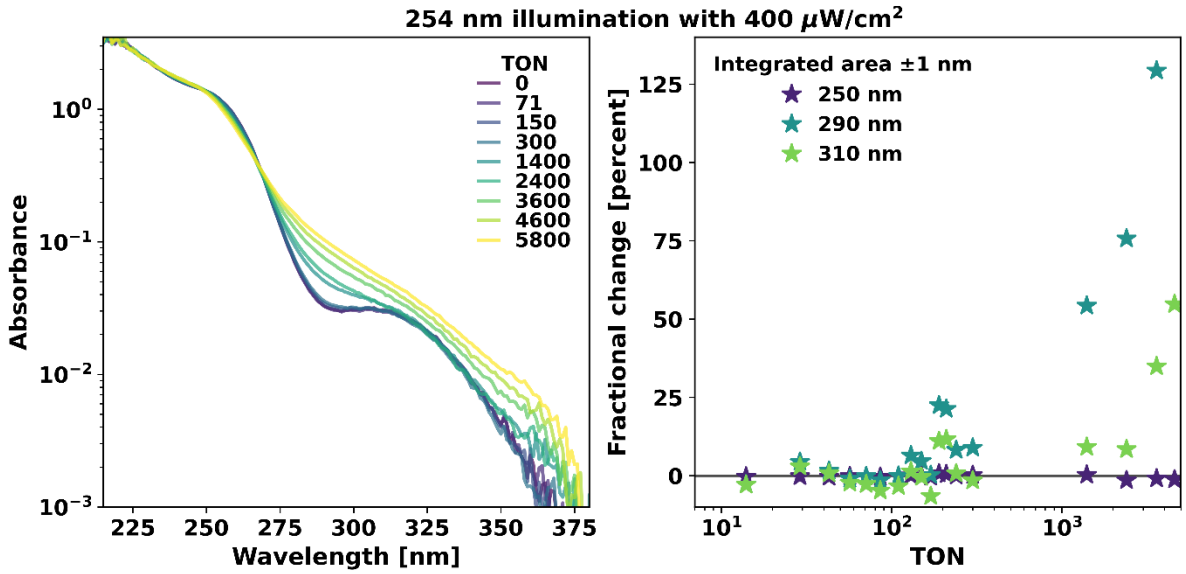

Figure S6: (left) absorption spectra of a sample of $[Co(PhB(MeIm)_3)_2]^+$ that was irradiated with UV light (254 nm) over the course of 80 hours. (right): Plot of fractional changes of the spectrum at the given wavelengths (averaged in a window ±1 nm).

To estimate the influence of oxygen on the sample, a previously sealed cuvette under nitrogen gas was opened and the sample solution was bubbled with ambient air. As can be seen from the absorption

spectra before and after aeration (Figure S7) oxygen does not have significant impact on the sample's absorption spectrum.

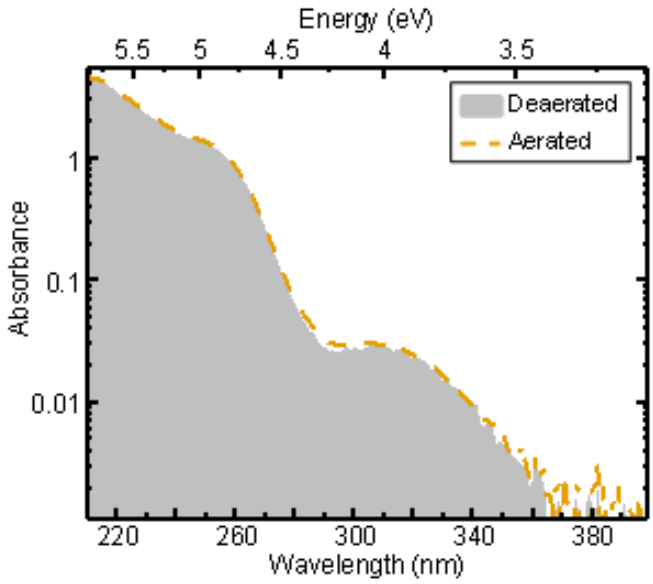

Figure S7: Influence of oxygen on the absorbance of $[Co(PhB(MeIm)_3)_2]^+$ plotted on semi-logarithmic scale. Sample was prepared at 0.725 mM concentration in deaerated acetonitrile under nitrogen atmosphere (grey area). For aeration the cuvette was opened and the solution bubbled with air (orange dashed line).

Luminescence quenching by oxygen

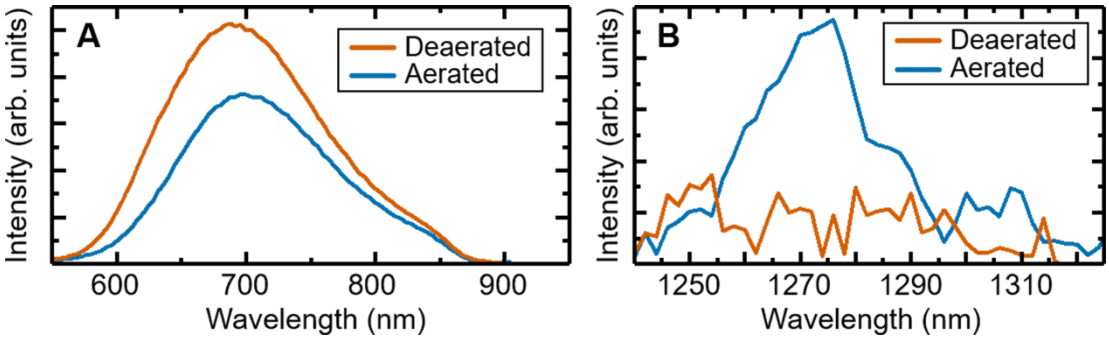

Figure S8: A) Changes of the emission spectra of $[Co(PhB(MeIm)_3)_2]^+$ at 750 µM concentration in acetonitrile with and without oxygen. B) Characteristic emission of $^1O_2$ recorded for the same sample as in A). The sample was prepared oxygen free (orange line), then shaken and bubbled with oxygen (blue line).

To investigate luminescence quenching by oxygen a sample of 0.75 µM $[Co(PhB(MeIm)_3)_2](PF_6)$ in acetonitrile was prepared. Deaeration was ensured by repeating three freeze-pump-thaw cycles under argon atmosphere. The sample was transferred into standard 1 cm optical path-length quartz cuvette (Hellma QS) under a flow of argon gas and the cuvette was sealed with a Teflon cap and parafilm. The emission spectrum of the pristine sample was recorded for 266 nm excitation (See orange trace in Figure S8 A). Subsequently oxygen was introduced to the sample by opening the cuvette, bubbling the sample solution with oxygen, shaking it and resealing again. The resulting emission spectrum is shown in blue in Figure S8 A. In the aerated solvent the emission intensity drops by ~30 % while the shape of the spectrum does not change. To further confirm that quenching by triplet oxygen is the cause for the decrease in emission intensity, we monitored the emission in the infrared region, too. The resulting spectra are given in Figure S8 B. For the deaerated sample no emission is observed, upon addition of

oxygen a new emission feature ~1268 nm arises. Emission at this wavelength can be associated to the transition of $^1\Delta_g$ to $^3\Sigma^-_g$ of O_2.[4]

Determination of the quantum yield

To determine the emission quantum yield (Φ) of $[Co(PhB(MeIm)_3)_2]^+$ we compare the emission intensity to a well know standard dye. For this we prepare a sample solution of $[Co(PhB(MeIm)_3)_2]^+$ in acetonitrile at 693 µM concentration. As reference we use 4-Dicyanomethylene-2-methyl-6-p-dimethylaminostyryl-4H-pyran (DCM) in dimethyl sulfoxide (DMSO) at 84 µM concentration. The latter was determined based on the molar absorption coefficient of DCM.[5] Using 308 nm excitation DCM has an Φ of 12 %.[6] For excitation of $[Co(PhB(MeIm)_3)_2]^+$ we use 266 nm, thus we first estimate the quantum yield of DCM for 266 nm excitation. This is done be exciting the same sample using the two different wavelengths while maintaining the rest of the experiment parameters. The resulting spectra are shown in Figure S9, along with the absorbance spectrum of the sample and the intensity spectrum of the lamp used for excitation. Integrating the spectra yields 2034 Counts/(Second·Pixel) and 342 Counts/(Second·Pixel) for 308 nm and 266 nm excitation, respectively. Given the quantum yield of 12 % and taking into account the difference in absorbance and excitation intensity this results in a quantum yield of 10.5 % for 266 nm excitation.

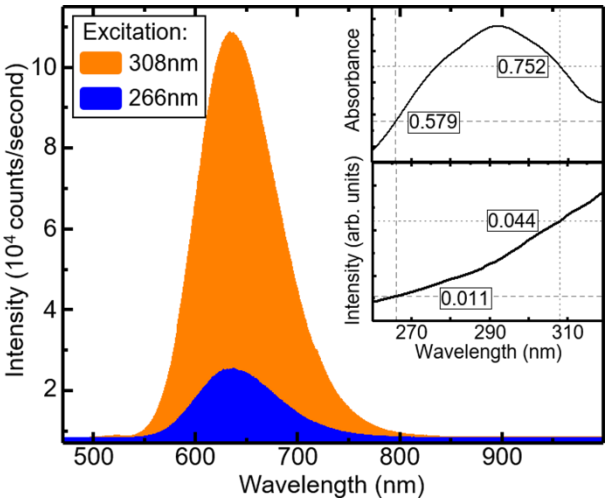

Figure S9: Emission spectrum of 4-Dicyanomethylene-2-methyl-6-p-dimethylaminostyryl-4H-pyran (DCM) in dimethyl sulfoxide (DMSO) at 84 µM concentration. For excitation at 266 nm (blue area) and 308 nm. Top Inset: Absorbance spectra of the respective samples with highlighted values at 266 nm and 308 nm. Bottom Inset: Intensity spectrum of the lamp used for excitation of the sample with highlighted values at 266 nm and 308 nm.

Next we compare the emission of DCM and $[Co(PhB(MeIm)_3)_2]^+$ for 266 nm excitation. The respective spectra are plotted in Figure S10. Integration of the spectra gives 1111 Counts/(Second·Pixel) for DCM and 8.2 Counts/(Second·Pixel) for $[Co(PhB(MeIm)_3)_2]^+$. Taking into account the higher absorbance of our sample this yields a ~4 orders of magnitude lower quantum yield, i.e., Φ = 0.01 %.

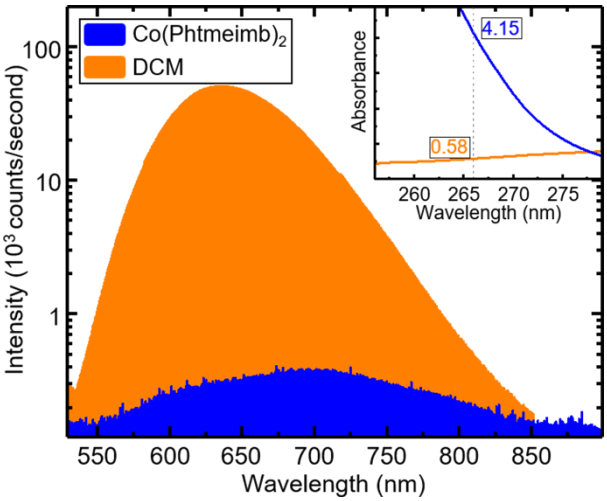

Figure S10: Emission spectrum of Co(phtmeimb)$_2$ in acetonitrile (blue area) and DCM in dimethyl sulfoxide (orange area) after excitation at 266 nm. Inset: Absorbance spectra of the respective samples with highlighted values at 266 nm.

Oscillator strength and transient molar absorption coefficients

To estimate the oscillator strength of the transitions observed in steady-state spectroscopy we apply a Gaussian fit to the measured absorption spectrum (Figure S11). The absorption features between 400 and 600 nm can only be seen in highly concentrated samples.

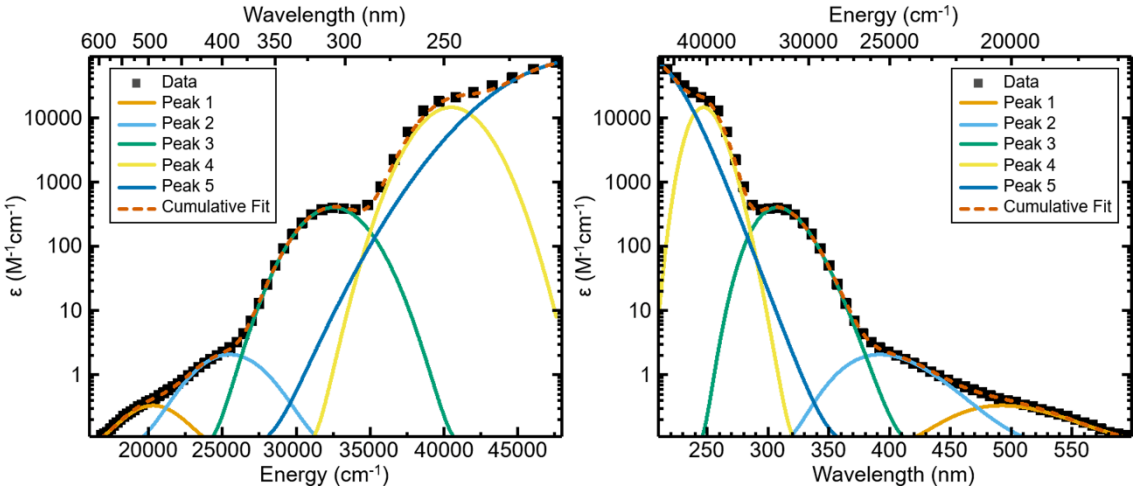

Figure S11: Measured molar absorption coefficient of [Co(PhB(MeIm)$_3$)$_2$]PF$_6$ in acetonitrile (black squares). Gaussian fits composed of five peaks (solid lines) and sum of all fits (dashed line). Fitting was performed on energy representation (left). For comparison the same plot versus wavelength is given (right).

From the fits we estimate the integrated molar absorption coefficient ($\int \varepsilon(\nu)\, d\nu$) and calculate the oscillator strength (f) based on:

$$f = 4.319 \cdot 10^{-9} \cdot \int \varepsilon(\nu)\, d\nu. \qquad 1$$

The resulting values are summarised in Table S2.

Table S2: Fit results, integrated molar absorption coefficient and calculated oscillator strength for steady-state absorption.

Peak	Centre	FWHM	Amplitude [M^{-1}cm^{-1}]	$\int \varepsilon(\nu)\, d\nu$ [M^{-1}cm^{-2}]	f
1	492 nm (20300 ± 15 cm^{-1})	110 ± 10.0 nm (4390 ± 570 cm^{-1})	0.28 ± 0.1	1.9·10^3 ± 1.3·10^3	8.6·10^{-6} ± 5.7·10^{-6}

2	392 nm (25500 ± 0 cm^{-1})	77 ± 1.0 nm (5010 ± 60 cm^{-1})	2.05 ± 0.1	$1.2 \cdot 10^4 \pm 1.1 \cdot 10^3$	$5.2 \cdot 10^{-5} \pm 4.8 \cdot 10^{-6}$
3	308 nm (32500 ± 0 cm^{-1})	42 ± 0.5 nm (4480 ± 1 cm^{-1})	400 ± 0.0	$1.9 \cdot 10^6 \pm 1.1 \cdot 10^3$	$8.2 \cdot 10^{-3} \pm 4.8 \cdot 10^{-6}$
4	247 nm (40500 ± 0 cm^{-1})	26 ± 0.0 nm (4325 ± 1 cm^{-1})	14500 ± 10.0	$6.7 \cdot 10^7 \pm 6.2 \cdot 10^4$	$2.9 \cdot 10^{-1} \pm 2.7 \cdot 10^{-4}$
5	202 nm (49600 ± 0 cm^{-1})	39 ± 0.0 nm (9420 ± 0 cm^{-1})	80000 ± 0.0	$8.0 \cdot 10^8 \pm 2.8 \cdot 10^3$	$3.5 \pm 1.2 \cdot 10^{-5}$

Next, we estimate the transition dipole moment (μ) and oscillator strength corresponding to the emissive transition. For a dipole in vacuum the dipole moment is given by the radiative rate (k_r) and the wavelength (λ_{max}) of the emission maximum via:

$$\mu = \sqrt{3\pi\varepsilon_0 \hbar k_r \left(\frac{1}{\lambda_{max}}\right)^3}. \quad 2$$

If we assume that all excited complexes end up in the emissive state then we can define the lower limit for the radiative rate, which is given by the quantum-yield (η) and the observed luminescence lifetime (τ_{PL}):

$$k_r = \frac{\eta}{\tau_{PL}}. \quad 3$$

From the transition dipole moment, we calculate the oscillator strength via:

$$f = \left(\frac{8\pi^2 m_e c}{3e^2 h}\right) \cdot \lambda_{max} \cdot \mu^2. \quad 4$$

Having the dipole moment and oscillator strength of the emissive transition calculated, it is tempting to construct a quantification of the emission that will allow us to directly compare the transition strength of emission and absorption using the common notation of molar absorption coefficient. Using Equation 1 we then calculate the integrated molar absorption coefficient corresponding to the oscillator strength of the emission. The resulting values are summarized in Table S3.

Table S3: Calculated parameters for the radiative transition.

η	τ_{PL}	λ_{max}	k_r	μ	f	$\int \varepsilon(\nu)\, d\nu$
0.0001	$8 \cdot 10^{-7}$ s	690 nm (14492 cm^{-1})	125 s^{-1}	0.18 D	$2.2 \cdot 10^{-4}$	$5.1 \cdot 10^4$ M^{-1}cm^{-2}

Although characterisation of a transition via oscillator strength or dipole moment is comprehensive, it is often handy to characterise the transition strength in conventional units of the molar absorption coefficient. To do that, we convert the measured spontaneous-emission spectrum into the stimulated-emission spectrum based on the Einstein coefficients for spontaneous (A_{21}) and stimulated emission (B_{21}):

$$A_{21} = \left(8\pi h \frac{\nu^3}{c^3}\right) B_{21} \quad 5$$

Afterwards, we scale the stimulated-emission spectrum so that the integral equals the calculated integrated molar absorption coefficient. The resulting spectrum is given in Figure S12. It gives the lower limit of the constructed molar absorption coefficient expected for the stimulated emission.

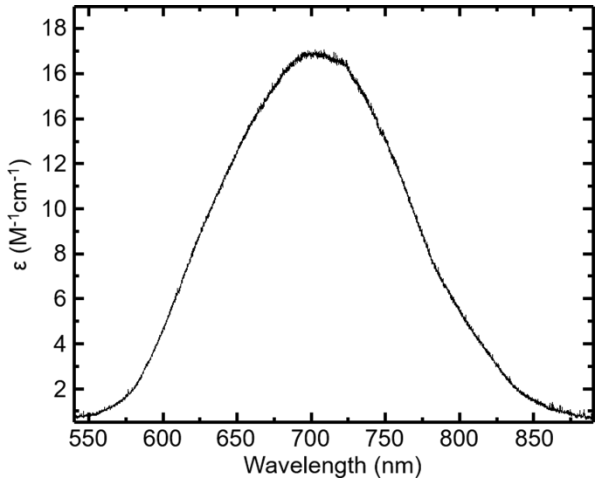

Figure S12: Calculated molar absorption coefficient spectrum of stimulated emission of $[Co(PhB(MeIm)_3)_2]PF_6$.

Next, we consider the influence of the assumption of the quantitative conversion of the initially excited population into the emissive long-lived state used in calculations of the transition strengths of ESA and SE. Apparently, if the conversion is less than 100% the ESA transition strength has to be larger to account for the same measured ΔA signal. Additionally, under the reduced conversion efficiency, the strength of the emissive transition should be larger than the evaluated above to result in the measured emission yield within the measured lifetime. In the experimental data, we have a qualitative indication of possible competitive energy relaxation pathways as the excitation spectrum does not coincide with the spectrum of steady-state absorption.

Estimation of ligand field splitting and Racah parameters

Based on the $3d^6$ electronic configuration of $[Co(PhB(MeIm)_3)_2]^+$ and the assumed strong ligand field splitting, we expect the three lowest energy absorption features to correspond to transitions from $^1A_{1g}$ to $^3T_{1g}$, $^3T_{2g}$, and $^1T_{1g}$ respectively. The energies of these transitions can be expressed in terms of ligand field splitting (10Dq) and Racah parameters (B and C). [7,8] Table S4 lists the transitions and respective energy expressions together with the assigned peaks (from Table S2) and the energies as well as molar absorption coefficients obtained by fitting the absorption spectrum.

The assignment of the three peaks is done based on the energy as well as the molar absorption coefficient. In terms of energy the sequence of involved states is choosen to fit according to the Tanabe-Sugano diagram for d^6 complexes with $\Delta/B > 4$, i.e. $^3T_{1g} < {}^3T_{2g} < {}^1T_{1g}$. The first two peaks show molar absorption coefficient in the range of 1 $M^{-1}cm^{-1}$ and below. This is attributed to spin-forbidden d-d transitions, thus we assign those to the transition involving $^3T_{1g}$ and $^3T_{2g}$. The third peak has a molar absorption coefficient in the 100 $M^{-1}cm^{-1}$ range that is typical for spin-allowed d-d transitions. Thus, we assign the third peak to the transition involving the $^1T_{1g}$.[7]

Table S4: Assignment of fitted peaks (Table S2) to transitions and corresponding energy expression in terms of 10Dq and Racah parameters.

Peak	Transition	Energy Expression	Energy [cm^{-1}]	Molar Absorption Coefficient [$M^{-1}cm^{-1}$]
1	$^1A_{1g} \rightarrow {}^3T_{1g}$	10Dq - 3C	20300	0.28 ± 0.1
2	$^1A_{1g} \rightarrow {}^3T_{2g}$	10Dq - 3C + 8B	25500	2.05 ± 0.1
3	$^1A_{1g} \rightarrow {}^1T_{1g}$	10Dq - C	32500	400 ± 0.0

The three transitions and corresponding energy expression result in a system of equations with three variables. Solving the equations yields ligand field splitting parameter of 10Dq=38600 cm^{-1} and Racah parameters of B=650 cm^{-1} and C=6100 cm^{-1}.

Transient absorption spectroscopy

The transient absorption (TA) experiments were carried out on two in-house build setups, both based on a Spitfire Pro XP (Spectra Physics) laser amplifier system that produces ~80 fs pulses at a central wavelength of 796 nm at 1 kHz repetition rate. The laser output is split into two parts i.e. to generate pump and probe beams. The delay between pump and probe beams is introduced by a computer-controlled delay stage (Aerotech) placed in the probe beam's path. The maximal achievable delay for this setup is ~10 ns. The pump beam (266 nm) is generated by frequency tripling the fundamental of the laser. For spectrally resolved transient absorption, a collinear optical parametric amplifier (TOPAS-C, Light Conversion) is used to generate the probe beam. The TOPAS generates a NIR beam, ~100 fs pulses with centre wavelength of 1350 nm that is focused onto a 5 mm CaF_2 crystal to generate a supercontinuum. After supercontinuum generation the probe pulses are split into two parts: the former overlapping with the pump pulse in the sample volume and the latter serving as a reference. The probe and the reference beams are then relayed onto the entrance slit of a prism spectrograph and dispersed onto a double photodiode array, each holding 512 elements (Pascher Instruments). The intensity of excitation pulses was set to 0.7 mW corresponding to ~10^{15} photons per pulse per cm^2 for a pump spot-size of ~$2 \cdot 10^{-3}$ cm^2. Mutual polarization between pump and probe beams was set to the magic angle (54.7°) by placing a Berek compensator in the pump beam. Time-resolution of the setup after dispersion correction is ≤150 fs.

To achieve longer pump-probe delays, single-colour transient absorption experiments were performed. Here, the probe was generated by a frequency doubled YAG laser triggered by the amplifier system and electronically delayed. Additionally, the detection was changed to single photodiodes for both probe and reference.

Samples were prepared by dissolving $[Co(PhB(MeIm)_3)_2]PF_6$ in MeCN. Sample solutions were then filled in 1 mm optical path length cuvettes (Hellma – Quartz Glass) and measurements performed at room temperature. To check for stability of the sample steady-state absorption spectra were measured before and after TA experiments. In some cases, after lengthy (~4 hours) measurements we noticed some changes in absorption spectra corresponding to between 300 and 1400 TON as presented on Fig. S6. Nevertheless, we have not observed any changes of the measured dynamics during the long data acquisitions within out S/N.

Time-resolved photoluminescence spectroscopy

Time-resolved photoluminescence (PL) was measured using an in house built setup based on the same laser-system as for TA experiments. For excitation of the sample either 266 nm (frequency tripled laser-fundamental) or 310 nm (generated by TOPAS) with the excitation density of ~10^{14} photons per pulse per cm^2 at both excitation wavelength was used. The sample was kept in a 1 cm quartz cuvette and excited in tilted front-face geometry. For detection, the luminescence was collected using a 2"-diameter lens with focal distance of 5 cm in ~7 cm distance to the sample to cover a larger solid-angle of emission. The magnified image of the sample was projected onto the entrance of a standard photomultiplier tube (PMT) equipped with three filters. A 575 nm long-pass colour-glass filter was used to supress scattered pump-light. Furthermore, two dielectric filters (Edmund Optics OD4 700 nm short-pass & 650 nm long-pass) were used to select the detection-wavelength window. The signal of the PMT was recorded using an oscilloscope (LeCroy WaveRunner 204MXi). As a typical measurement took only took several minutes, no sample degradation is expected in these experiments.

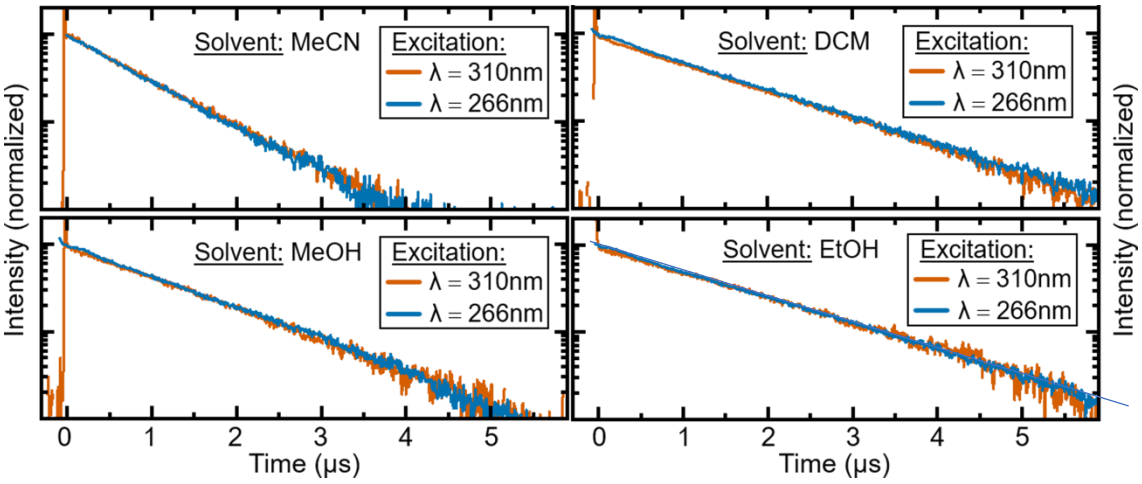

Figure S13: Photoluminescence transients of $[Co(PhB(MeIm)_3)_2]PF_6$ in different solvents for 310 nm (orange) and 266 nm (blue) excitation. For comparison all transients have been normalized.

Using this setup, the room temperature time-resolved photoluminescence of $[Co(PhB(MeIm)_3)_2]PF_6$ in 4 different solvents was measured. The solvents were: Acetonitrile (MeCN), Dichloromethane (CH_2Cl_2), Methanol (MeOH), and Ethanol (EtOH). The resulting transients for both excitation wavelengths are given in Figure S13. Besides a strong artefact around time-zero for the 266 nm excitation the decay for both excitation wavelength is virtually identical. This is also reflected in the lifetimes obtained by fitting a single-exponential decay to the data. The resulting lifetimes and sample concentrations are given in Table S5.

Table S5: Sample concentrations of $[Co(PhB(MeIm)_3)_2]PF_6$ in different solvents and lifetimes obtained by single-exponential fits to the PL transients.

Solvent	Sample concentration	Single exponential lifetime (266 nm excitation)	Single exponential lifetime (310 nm excitation)
MeCN	220 µM	0.84 µs	0.82 µs
CH_2Cl_2	230 µM	1.41 µs	1.37 µs
MeOH	120 µM	1.26 µs	1.25 µs
EtOH	95 µM	1.58 µs	1.49 µs

(Spectro)electrochemistry

Electrochemical data in MeCN shows that $[Co(PhB(MeIm)_3)_2]^+$ undergoes one reversible (0.96 V vs. Fc^+/Fc) and two irreversible (1.55 and 1.76 V vs. Fc^+/Fc) oxidations (Figure S14). The reversible oxidation is assigned to the Co(IV/III) couple while the irreversible oxidations are close to the reported value for ligand oxidation of the analogue Fe complex (1.67 V vs. Fc^+/Fc),[2] however, formation of an instable Co(V) species cannot be excluded. Notably no reduction signals were found in the potential window of MeCN (-3 V vs Fc^+/Fc) showing high stability of the Co(III) species over more than 4 V. This is in accordance with the findings for the analogue Fe compound, where no further reduction than to the t_{2g}^6 Fe(II) could be observed and ligand reduction was estimated to occur at more negative potentials than -3.3 V vs. Fc^+/Fc.[2]

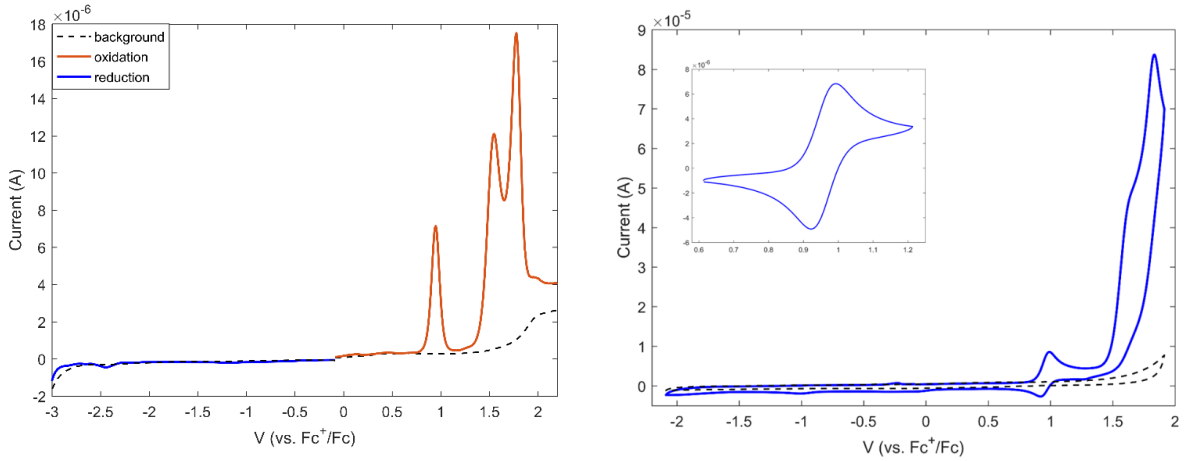

Figure S14: A) Differential pulse and B) cyclic voltammograms of $[Co(PhB(MeIm)_3)_2]^+$ (1.3 mM) in acetonitrile (0.1 M NBu_4PF_6).

When a potential of 1.2V is applied in spectroelectrochemical investigations the appearance of absorption bands at 450, 600 and 1516 nm is observed (Figure S15). The latter can be assigned to an LMCT transition as the energy (≈0.8 eV) roughly corresponds to the difference in potential between Co(IV/III) and the 2nd irreversible oxidation, tentatively assigned to ligand oxidation.

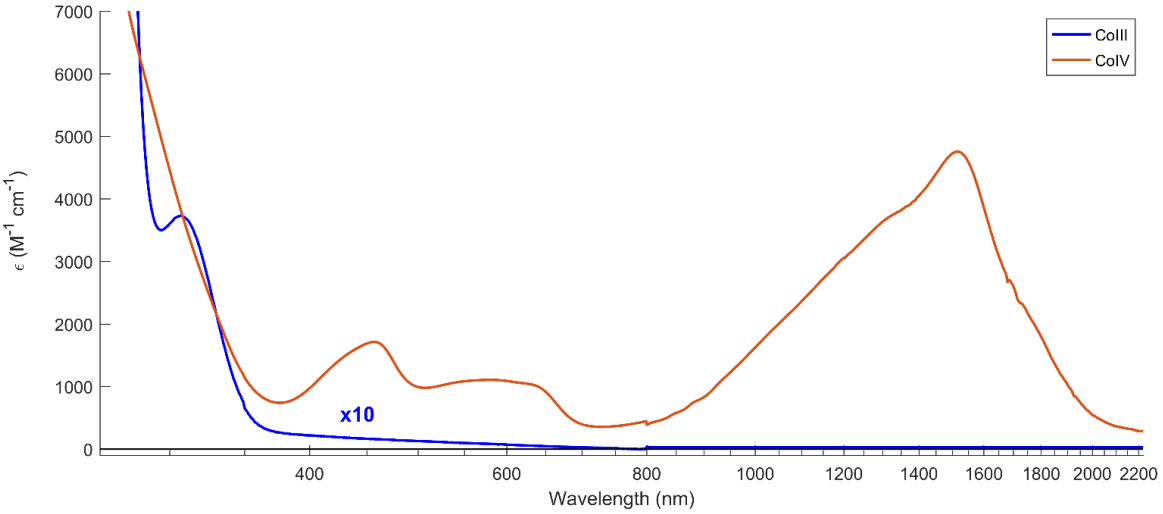

Figure S15: Spectra of $[Co(PhB(MeIm)_3)_2]^+$ and electrochemically generated $[Co(PhB(MeIm)_3)_2]^{2+}$.

Single crystal X-ray diffraction

Crystals of suitable quality were obtained by slow evaporation of a solution of $[Co(PhB(MeIm)_3)_2]PF_6$ in MeCN/toluene (1:2). A single crystal of $[Co(PhB(MeIm)_3)_2]PF_6$ covered in paratone oil was mounted on a MiTeGen micro-mount loop and rapidly transferred to the nitrogen cold stream of the diffractometer. Data collection was performed at 110(2) K on an Agilent Xcalibur Sapphire3 diffractometer equipped with a Mo *Kα* high-brilliance I*μ*S radiation source (*λ* = 0.71073 Å) and an Oxford Cryosystems low temperature device. Absorption was corrected for using multi-scan empirical absorption correction with spherical harmonics as implemented in the SCALE3 ABSPACK scaling algorithm.[8] The structure was solved in WinGX[9] using SUPERFLIP[10] and refined using SHELXL 2016/4.[11] Non-hydrogen atoms were refined anisotropically.

Table S6: Crystal data for compound $[Co^{III}(PhB(MeIm)_3)_2]PF_6$. [a]

Chemical formula	$2(C_{36}H_{40}B_2CoN_{12})$, $2(PF_6)$, $3(C_7H_8)$	
Formula Mass	1824.77	
Crystal size /mm^3	0.5 x 0.5 x 0.1	
Crystal habit	colourless, block	
Crystal system	Triclinic	
Unit cell dimensions:	*a* = 9.8868(3) Å	*α* = 91.166(3) °
	b = 11.3094(5) Å	*β* = 94.315(3) °
	c = 19.5352(7) Å	*γ* = 90.523(3) °
Unit cell volume /Å^3	2177.54(14)	
Collection temperature/K	110(2)	
Space group	*P*-1	
Number of formula units per cell, *Z*	1	
Radiation type	MoKa	
Absorption coefficient, m/mm^{-1}	0.501	
No. reflections measured	25057	
No. independent reflections	10088	
R_{int}	0.0411	
Final R_1 values *(I >2σ(I))*	0.0511	
Final R_1 values *(all data)*	0.0705	
Final $wR(F^2)$ values *(I >2σ(I))*	0.1076	
Goodness of fit on F^2	1.020	
Largest diff. peak and hole /e-/Å^3	0.519 and -0.427	
CCDC	1956887	

[a] A model could not be found for a disordered moiety which was instead removed with SQUEEZE. The resulting void contained 53 electrons. The PF_6^- ion was modelled with SIMU and DELU restrains as disordered over three positions with a refined occupancy of 0.65 : 0.21 : 0.14.

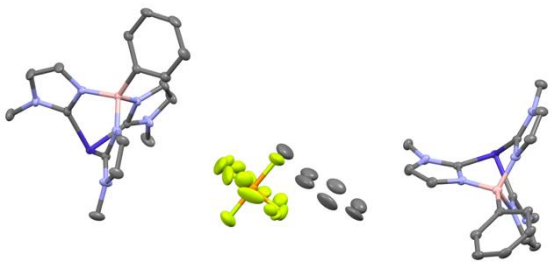

Figure S16: The asymmetric unit of $[Co^{III}(PhB(MeIm)_3)_2]PF_6$. Thermal ellipsoids are shown at 50% probability. Gray = carbon atom; light blue = nitrogen atom; pink = boron atom; dark blue = cobalt atom; orange = phosphorous atom; green = fluorine atom. Hydrogen atoms are omitted for clarity.

Quantum Chemistry

Fully relaxed singlet, triplet and quintet states of Co complex were all optimized using restricted or unrestricted density functional theory (DFT) calculations as appropriate. All minima were confirmed by frequency analysis. Acetonitrile solvent was included by the polarizable continuum model (PCM). A superfine integral grid was also used for all calculations. The fully relaxed geometries of each spin were used to perform subsequent single point calculations for the singlet, triplet and quintet states in order to construct the energy profile in Figure 4. Time dependent DFT (TD-DFT) singlet and triplet excited state calculations were also carried out and used to identify the lowest MC and CT states. All reported calculations were performed with the modified B3LYP hybrid functional,[12] B3LYP*[13] together with the standard 6-311G(d) basis set[14,15] for all atoms using the Gaussian09 package Revision E. 01.[16]

Table S7: Calculated relative energies (E_{rel}) of the $[Co(PhB(MeIm)_3)_2]^{+1}$ metal complex for average Co-C bond distances (R_{av}). Energy values reported for the singlet, triplet and quintet states of the ground state (GS), metal center states (MC) and charge transfer states (CT) for both DFT and TD-DFT methodologies.

	DFT E_{rel} (eV)			TD-DFT E_{rel} (eV)			
R_{av} Co-C (Å)	**GS**	**^{3}MC**	**^{5}MC**	**^{1}MC**	**^{1}CT**	**^{3}MC**	**^{3}CT**
1.98	0.00	2.94	5.33	3.63	4.76	3.02	4.40
2.10	0.75	2.11	4.23	3.04	4.68	2.22	4.33
2.18	1.29	2.77	3.67	3.49	5.28	2.69	4.92

Table S8: Computational values from TD-DFT calculations for the absorption and emission energies and wavelengths (λ) and oscillator strengths (f) of the $[Co(PhB(MeIm)_3)_2]^{+1}$ metal complex. The ΔSCF emission energy value at DFT level methodologies.

	λ (nm)	**Energy (eV)**	**f**
Absorption (GS→^{1}MC)	341	3.63	
Absorption (GS→^{1}CT)	261	4.76	$1.4.10^{-2}$
Emission (^{3}MC→GS)	847	1.46	
ΔSCF Emission (^{3}MC→GS)*	917	1.35	

Table S9: Singlet TD-DFT vertical excitations for the first 12 root of $[Co(PhB(MeIm)_3)_2]^{+1}$ at Co-C average distance of 1.98 Å together with the wavelength (λ), oscillator strength (f) , electronic transitions and corresponding coefficients and type of transition.

State	**Spin**	**Energy (eV)**	**λ (nm)**	**f**	**Transition**	**Coefficient**	**Assignment**
1	Singlet	3.6323	341.34	0.0000	HOMO-13 → LUMO+4 HOMO-13 → LUMO+8 HOMO-6 → LUMO+4 HOMO-1 → LUMO+2	0.209 0.111 0.143 -0.150	MC

					HOMO-1 → LUMO+4	0.510	
					HOMO-1 → LUMO+8	0.235	
					HOMO → LUMO+5	-0.182	
					HOMO → LUMO+6	-0.140	
					HOMO-14 → LUMO+5	0.145	
					HOMO-14 → LUMO+6	0.107	
					HOMO-12 → LUMO+5	0.109	
					HOMO-6 → LUMO+4	0.318	
2	Singlet	3.7703	328.85	0.0000	HOMO-6 → LUMO+8	0.151	MC
					HOMO-1 → LUMO+4	0.113	
					HOMO → LUMO+5	0.432	
					HOMO → LUMO+6	0.300	
					HOMO → LUMO+10	-0.101	
					HOMO-14 → LUMO+4	0.127	
					HOMO-13 → LUMO+5	-0.107	
					HOMO-6 → LUMO+5	0.271	
					HOMO-6 → LUMO+6	0.204	
3	Singlet	3.7885	327.26	0.0000	HOMO-1 → LUMO+5	-0.254	MC
					HOMO-1 → LUMO+6	-0.174	
					HOMO → LUMO+2	-0.117	
					HOMO → LUMO+4	0.406	
					HOMO → LUMO+8	0.197	
					HOMO-13 → LUMO+5	0.120	
					HOMO-13 → LUMO+6	0.117	
4	Singlet	4.2566	291.27	0.0000	HOMO-1 → LUMO+5	0.384	MC
					HOMO-1 → LUMO+6	0.326	
					HOMO → LUMO+2	-0.152	
					HOMO → LUMO+4	0.389	
					HOMO-6 → LUMO+2	0.165	
					HOMO-6 → LUMO+4	-0.497	
					HOMO-6 → LUMO+8	-0.145	
5	Singlet	4.3792	283.12	0.0000	HOMO-1 → LUMO+4	0.192	MC
					HOMO-1 → LUMO+8	0.165	
					HOMO → LUMO+1	0.107	
					HOMO → LUMO+5	0.323	
					HOMO-6 → LUMO+5	-0.397	
					HOMO-6 → LUMO+6	-0.380	
					HOMO-6 →LUMO+10	0.116	
6	Singlet	4.5129	274.73	0.0000	HOMO-1 → LUMO+1	-0.120	MC
					HOMO-1 → LUMO+5	-0.297	
					HOMO → LUMO+4	0.142	
					HOMO → LUMO+8	0.207	

7	Singlet	4.7125	263.10	0.0000	HOMO-6 → LUMO+4 HOMO-1 → LUMO+8 HOMO → LUMO+1 HOMO → LUMO+6	-0.107 0.125 -0.641 0.188	CT
8	Singlet	4.7206	262.64	0.0045	HOMO-3 → LUMO+1 HOMO → LUMO HOMO → LUMO+7	-0.107 -0.683 0.138	CT
9	Singlet	4.7572	260.63	0.0143	HOMO-1 → LUMO HOMO-1 → LUMO+7	0.690 -0.114	CT
10	Singlet	4.7797	259.40	0.0000	HOMO-1 → LUMO+1	-0.670	CT
11	Singlet	4.8657	254.81	0.0000	HOMO-1 → LUMO+2 HOMO-1 → LUMO+8 HOMO → LUMO+1	0.600 0.287 0.140	CT
12	Singlet	4.8926	253.41	0.0000	HOMO-3 → LUMO+2 HOMO → LUMO+3	-0.101 0.694	CT

Table S10: Triplet TD-DFT vertical excitations for the first 12 root of $[Co(PhB(MeIm)_3)_2]^{+1}$ at Co-C average distance of 1.98 Å together with the wavelength (λ), oscillator strength (f) , electronic transitions and corresponding coefficients and type of transition.

State	**Spin**	**Energy (eV)**	**λ (nm)**	**f**	**Transition**	**Coefficient**	**Assignment**
1	Triplet	3.0183	410.77	0.0000	HOMO-13 → LUMO+4 HOMO-13 → LUMO+8 HOMO-6 → LUMO+4 HOMO-1 → LUMO+2 HOMO-1 → LUMO+4 HOMO-1 → LUMO+8 HOMO → LUMO+5	0.260 0.140 0.125 -0.147 0.519 0.251 -0.102	MC
2	Triplet	3.1048	399.33	0.0000	HOMO-14 → LUMO+4 HOMO-14 → LUMO+8 HOMO-12 → LUMO+4 HOMO-6 → LUMO+5 HOMO-6 → LUMO+6 HOMO-1 → LUMO+5 HOMO-1 → LUMO+6 HOMO → LUMO+2 HOMO → LUMO+4 HOMO → LUMO+8	0.200 0.102 0.149 0.137 0.108 -0.163 -0.105 -0.146 0.499 0.227	MC

3	Triplet	3.1533	393.18	0.0000	HOMO-14 → LUMO+5 -0.179 HOMO-14 → LUMO+6 -0.139 HOMO-12 → LUMO+5 -0.133 HOMO-12 → LUMO+6 -0.103 HOMO-6 → LUMO+4 -0.271 HOMO-6 → LUMO+8 -0.134 HOMO → LUMO+5 -0.434 HOMO → LUMO+6 -0.325 HOMO → LUMO+10 0.112	MC
4	Triplet	3.2995	375.76	0.0000	HOMO-13 → LUMO+5 0.217 HOMO-13 → LUMO+6 0.172 HOMO-6 → LUMO+5 -0.109 HOMO-1 → LUMO+5 0.446 HOMO-1 → LUMO+6 0.339 HOMO-1 → LUMO+10 -0.111 HOMO → LUMO+4 0.207	MC
5	Triplet	3.3711	367.78	0.0000	HOMO-6 → LUMO+2 -0.149 HOMO-6 → LUMO+4 0.528 HOMO-6 → LUMO+8 0.254 HOMO-1 → LUMO+4 -0.150 HOMO → LUMO+5 -0.209 HOMO → LUMO+6 -0.143	MC
6	Triplet	3.4904	355.21	0.0000	HOMO-6 → LUMO+5 -0.507 HOMO-6 → LUMO+6 -0.404 HOMO-6 → LUMO+10 0.142 HOMO-1 → LUMO+5 -0.150	MC
7	Triplet	3.8491	322.12	0.0000	HOMO-10 → LUMO+3 0.303 HOMO-9 → LUMO+2 0.290 HOMO-8 → LUMO -0.110 HOMO-8 → LUMO+1 0.349 HOMO-7 → LUMO -0.350 HOMO-7 → LUMO+1 0.110	$\pi \rightarrow \pi^*$
8	Triplet	3.8491	322.12	0.0000	HOMO-10 → LUMO+2 -0.289 HOMO-9 → LUMO+3 -0.304 HOMO-8 → LUMO 0.349 HOMO-8 → LUMO+1 0.110 HOMO-7 → LUMO -0.110 HOMO-7 → LUMO+1 -0.351	$\pi \rightarrow \pi^*$
9	Triplet	4.3169	287.20	0.0000	HOMO-4 → LUMO -0.121 HOMO-4 → LUMO+7 0.210 HOMO-3 → LUMO+9 -0.101 HOMO-2 → LUMO+4 -0.113	MC

					HOMO-1 → LUMO+1	0.293	
					HOMO-1 → LUMO+5	0.287	
					HOMO-1 → LUMO+6	-0.367	
					HOMO → LUMO+2	0.108	
					HOMO → LUMO+8	0.210	
					HOMO-5 → LUMO+9	0.163	
					HOMO-3 → LUMO+3	0.131	
					HOMO-3 → LUMO+9	0.173	
					HOMO-3 → LUMO+13	0.138	
					HOMO-3 → LUMO+14	-0.118	
					HOMO-2 → LUMO+2	0.161	
10	Triplet	4.4021	281.65	0.0000	HOMO-2 → LUMO+4	-0.158	MC
					HOMO-2 → LUMO+8	0.114	
					HOMO-2 → LUMO+11	0.112	
					HOMO → LUMO+2	-0.276	
					HOMO → LUMO+8	-0.324	
					HOMO → LUMO+11	-0.124	
					HOMO → LUMO+16	0.142	
					HOMO-5 → LUMO	-0.123	
					HOMO-5 → LUMO+7	0.220	
					HOMO-4 → LUMO+9	0.117	
					HOMO-4 → LUMO+13	-0.155	
					HOMO-3 → LUMO+7	-0.138	
					HOMO-2 → LUMO+1	0.182	
					HOMO-2 → LUMO+5	0.186	
11	Triplet	4.4056	281.43	0.0000	HOMO-2 → LUMO+6	-0.229	CT
					HOMO-1 → LUMO+2	0.105	
					HOMO-1 → LUMO+4	-0.104	
					HOMO-1 → LUMO+8	0.190	
					HOMO-1 → LUMO+16	0.119	
					HOMO → LUMO+1	0.198	
					HOMO → LUMO+5	0.158	
					HOMO → LUMO+6	-0.216	
					HOMO-5 → LUMO+1	-0.131	
					HOMO-5 → LUMO+5	-0.145	
					HOMO-5 → LUMO+6	0.182	
					HOMO-4 → LUMO+4	0.214	
12	Triplet	4.4125	280.98	0.0000	HOMO-4 → LUMO+16	-0.141	$\pi \rightarrow \pi^*$
					HOMO-3 → LUMO+6	-0.137	
					HOMO-2 → LUMO	0.213	
					HOMO-2 → LUMO+7	-0.324	
					HOMO-1 → LUMO+9	-0.144	
					HOMO-1 → LUMO+13	0.176	

HOMO	→ LUMO	0.140
HOMO	→ LUMO+7	-0.167

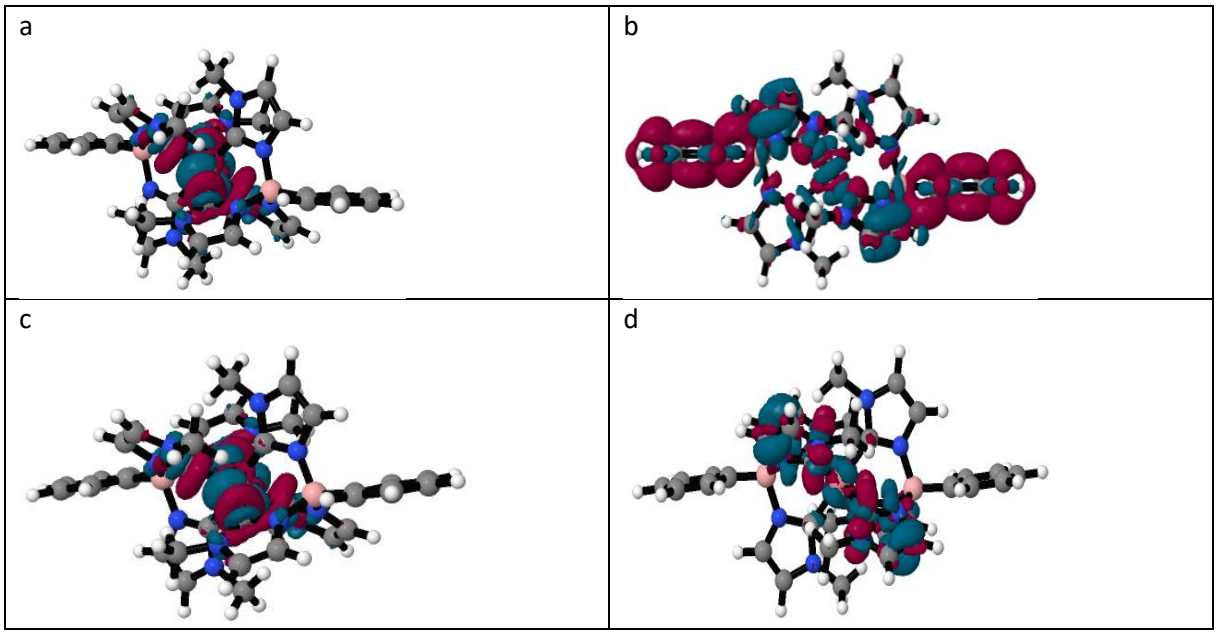

Figure S17: Selected electron density difference (EDD) plots between ground state and selected key excited states (ES) of $[Co(PhB(MeIm)_3)_2]^+$ at the relaxed ground state geometry with Co-C average distance of 1.98 Å at TD-DFT level. Depletion of density is coloured in blue and gain of density is coloured in red. An isovalue of 0.001 was used for plotting all density differences contours. The EDD results shown are for a) singlet excited state 1 assigned as mainly ^{1}MC character, b) singlet excited state 9 assigned as mainly ^{1}CT character, c) triplet excited state 1 assigned as mainly ^{3}MC character, and d) triplet excited state 11 assigned as mainly ^{3}CT character.

Table S11: Singlet TD-DFT vertical excitations for the first 12 root of $[Co(PhB(MeIm)_3)_2]^{+1}$ at Co-C average distance of 2.10 Å together with the wavelength (λ), oscillator strength (f) , electronic transitions and corresponding coefficients and type of transition.

State	Spin	Energy (eV)	λ (nm)	f	Transition	Coefficient	Assignment
1	Singlet	2.2904	541.32	0.0000	HOMO-11 → LUMO	0.324	MC
					HOMO-8 → LUMO	0.100	
					HOMO-6 → LUMO	-0.169	
					HOMO-3 → LUMO	0.299	
					HOMO-1 → LUMO	0.494	
2	Singlet	2.4205	512.22	0.0000	HOMO-12 → LUMO	0.226	MC
					HOMO-8 → LUMO	0.171	
					HOMO-6 → LUMO	-0.302	
					HOMO-3 → LUMO	-0.135	
					HOMO → LUMO	0.525	
3	Singlet	2.9263	423.70	0.0000	HOMO-8 → LUMO	-0.286	MC
					HOMO-6 → LUMO	0.472	

					HOMO-1 → LUMO	0.206	
					HOMO → LUMO	0.347	
					HOMO-12 →LUMO+5		
					HOMO-8 → LUMO+5	0.220	
					HOMO-6 → LUMO+5	-0.126	
4	Singlet	3.4658	357.74	0.0000	HOMO-1 → LUMO+5	0.195	MC
					HOMO → LUMO+3	0.224 0.187	
					HOMO → LUMO+5	0.474 0.113	
					HOMO → LUMO+7		
					HOMO-3 → LUMO	0.547	
5	Singlet	3.7737	328.54	0.0000	HOMO-1 → LUMO	-0.382	MC
					HOMO → LUMO	0.198	
6	Singlet	3.8420	322.70	0.0038	HOMO-4 → LUMO	0.301	CT
					HOMO-2 → LUMO	0.630	
					HOMO-5 → LUMO	-0.132	
7	Singlet	3.9265	315.76	0.0552	HOMO-4 → LUMO	0.628	CT
					HOMO-2 → LUMO	-0.283	
					HOMO-11 → LUMO+5	0.228	
					HOMO-6 → LUMO	-0.107	
					HOMO-6 → LUMO+5	0.148	
					HOMO-3 → LUMO+3	0.104	
					HOMO-3 → LUMO+5	0.261	
8	Singlet	3.9766	311.79	0.0000	HOMO-1 → LUMO+3	0.147	MC
					HOMO-1 → LUMO+5	0.387	
					HOMO-1 → LUMO+7	0.119	
					HOMO → LUMO+3	-0.118 -	
					HOMO → LUMO+5	0.249	
					HOMO-5 → LUMO	0.682	
9	Singlet	4.0311	307.57	0.0098	HOMO-2 → LUMO	-0.135	CT
					HOMO-11 → LUMO	0.118	
					HOMO-11 → LUMO+5	-0.102	
					HOMO-8 → LUMO+3	-0.104	
					HOMO-8 → LUMO+5	-0.254	
					HOMO-6 → LUMO+3	0.176	
10	Singlet	4.2074	294.68	0.0000	HOMO-6 → LUMO+5	0.431	MC
					HOMO-6 → LUMO+7	0.149	
					HOMO-3 → LUMO	-0.158	
					HOMO-1 → LUMO+5	-0.222	
					HOMO → LUMO+5	-0.123	

11	Singlet	4.4613	277.91	0.0000	HOMO-11 → LUMO HOMO-6 → LUMO+5 HOMO-3 → LUMO HOMO-1 → LUMO	0.581 -0.130 -0.237 -0.196	MC
12	Singlet	4.6091	269.00	0.0000	HOMO-12 → LUMO HOMO-9 → LUMO HOMO-8 → LUMO HOMO-1 → LUMO HOMO → LUMO	0.551 -0.197 -0.229 -0.108 -0.204	MC

Table S12: Triplet TD-DFT vertical excitations for the first 12 root of $[Co(PhB(MeIm)_3)_2]^{+1}$ at Co-C average distance of 2.10 Å together with the wavelength (λ), oscillator strength (f) , electronic transitions and corresponding coefficients and type of transition.

State	Spin	Energy (eV)	λ (nm)	f	Transition	Coefficient	Assignment
1	Triplet	1.4645	846.58	0.0000	HOMO-11 → LUMO HOMO-3 → LUMO HOMO-1 → LUMO	0.378 0.305 0.501	MC
2	Triplet	1.5312	809.73	0.0000	HOMO-12 → LUMO HOMO-11 → LUMO HOMO-6 → LUMO HOMO-3 → LUMO HOMO → LUMO	0.323 -0.105 -0.152 -0.143 0.575	MC
3	Triplet	1.7792	696.84	0.0000	HOMO-8 → LUMO HOMO-6 → LUMO HOMO-1 → LUMO HOMO → LUMO	-0.349 0.579 0.112 0.153	MC
4	Triplet	2.7881	444.69	0.0000	HOMO-12 → LUMO+3 HOMO-12 → LUMO+5 HOMO-6 → LUMO+5 HOMO-1 → LUMO+5 HOMO → LUMO+3 HOMO → LUMO+5 HOMO → LUMO+7	0.110 0.280 0.120 0.230 0.192 0.482 0.138	MC
5	Triplet	2.9602	418.83	0.0000	HOMO-11 → LUMO+3 HOMO-11 → LUMO+5 HOMO-3 → LUMO+3 HOMO-3 → LUMO+5 HOMO-1 → LUMO+3 HOMO-1 → LUMO+5	0.126 0.320 0.115 0.289 0.153 0.385	MC

					HOMO-1 → LUMO+7	0.111	
					HOMO → LUMO+5	-0.195	
6	Triplet	3.1621	392.10	0.0000	HOMO-8 → LUMO+3	-0.120	MC
					HOMO-8 → LUMO+5	-0.302	
					HOMO-6 → LUMO+3	0.202	
					HOMO-6 → LUMO+5	0.509	
					HOMO-6 → LUMO+7	0.160	
					HOMO-1 → LUMO+5	-0.108	
7	Triplet	3.5252	351.71	0.0000	HOMO-22 → LUMO	0.462	MC
					HOMO-3 → LUMO	0.418	
					HOMO-1 → LUMO	-0.238	
					HOMO → LUMO	0.149	
8	Triplet	3.5798	346.35	0.0000	HOMO-14 → LUMO	-0.202	CT
					HOMO-5 → LUMO	0.308	
					HOMO-4 → LUMO	0.505	
					HOMO-2 → LUMO	-0.277	
9	Triplet	3.7497	330.65	0.0000	HOMO-5 → LUMO	0.240	CT
					HOMO-4 → LUMO	0.186	
					HOMO-2 → LUMO	0.621	
10	Triplet	3.8055	325.81	0.0000	OMO-22 → LUMO	-0.486	MC
					HOMO-3 → LUMO	0.385	
					HOMO-1 → LUMO	-0.271	
					HOMO → LUMO	0.117	
11	Triplet	3.8383	323.02	0.0000	HOMO-5 → LUMO	0.552	CT
					HOMO-4 → LUMO	-0.410	
12	Triplet	3.8473	322.27	0.0000	HOMO-10 → LUMO+4	-0.308	$\pi \rightarrow \pi^*$
					HOMO-9 → LUMO+3	0.282	
					HOMO-9 → LUMO+5	-0.125	
					HOMO-8 → LUMO+2	0.309	
					HOMO-7 → LUMO+1	0.363	
					HOMO-7 → LUMO+6	0.104	
					HOMO-6 → LUMO+2	0.186	

Table S13: Singlet TD-DFT vertical excitations for the first 12 root of $[Co(PhB(MeIm)_3)_2]^{+1}$ at Co-C average distance of 2.18 Å together with the wavelength (λ), oscillator strength (f) , electronic transitions and corresponding coefficients and type of transition.

State	Spin	Energy (eV)	λ (nm)	f	Transition	Coefficient	Assignment
1	Singlet	2.2007	563.40	0.0000	HOMO-11 → LUMO	0.332	MC
					HOMO-8 → LUMO	0.179	

					HOMO-1 → LUMO	0.554	
					HOMO → LUMO+1	-0.158	
2	Singlet	2.3829	520.31	0.0000	HOMO-12 → LUMO+1	0.293	MC
					HOMO-8 → LUMO	0.369	
					HOMO-7 → LUMO	0.157	
					HOMO → LUMO+1	0.483	
3	Singlet	2.3880	519.21	0.0000	HOMO-12 → LUMO	0.248	MC
					HOMO-11 → LUMO+1	-0.143	
					HOMO-8 → LUMO+1	0.347	
					HOMO-7 → LUMO+1	0.142	
					HOMO-1 → LUMO+1	-0.275	
					HOMO → LUMO	0.432	
4	Singlet	2.9833	415.59	0.0000	HOMO-12 → LUMO	0.178	MC
					HOMO-11 → LUMO+1	0.215	
					HOMO-8 → LUMO+1	-0.178	
					HOMO-1 → LUMO+1	0.456	
					HOMO → LUMO	0.412	
5	Singlet	3.0944	400.67	0.0000	HOMO-12 → LUMO+1	-0.149	MC
					HOMO-8 → LUMO	0.499	
					HOMO-7 → LUMO	0.209	
					HOMO-1 → LUMO	-0.264	
					HOMO → LUMO+1	-0.325	
6	Singlet	3.2952	376.25	0.0000	HOMO-11 → LUMO+1	0.166	MC
					HOMO-8 → LUMO+1	0.515	
					HOMO-7 → LUMO+1	0.222	
					HOMO-1 → LUMO+1	0.347	
					HOMO → LUMO	-0.174	
7	Singlet	3.7909	327.06	0.0000	HOMO-2 → LUMO	0.691	CT
					HOMO → LUMO	-0.143	
8	Singlet	3.9191	316.36	0.0060	HOMO-5 → LUMO	-0.220	CT
					HOMO-3 → LUMO	0.670	
9	Singlet	3.9446	314.31	0.0036	HOMO-5 → LUMO+1	0.133	CT
					HOMO-4 → LUMO	0.682	
10	Singlet	3.9887	310.84	0.0464	HOMO-5 → LUMO	0.656	CT
					HOMO-4 → LUMO+1	0.134	
					HOMO-3 → LUMO	0.215	
11	Singlet	4.0258	307.98	0.0000	HOMO-2 → LUMO+1	0.688	CT
					HOMO → LUMO+1	-0.152	

12	Singlet	4.1446	299.15	0.0033	HOMO-5 → LUMO+1 HOMO-3 → LUMO+1	0.189 0.669	CT

Table S14: Triplet TD-DFT vertical excitations for the first 12 root of $[Co(PhB(MeIm)_3)_2]^{+1}$ at Co-C average distance of 2.18 Å together with the wavelength (λ), oscillator strength (f) , electronic transitions and corresponding coefficients and type of transition.

State	Spin	Energy (eV)	λ (nm)	f	Transition	Coefficient	Assignment
1	Triplet	1.4063	881.65	0.0000	HOMO-11 → LUMO HOMO-8 → LUMO HOMO-1 → LUMO HOMO-1 → LUMO	0.393 0.110 0.575 0.111	MC
2	Triplet	1.5214	814.93	0.0000	HOMO-12 → LUMO HOMO-8 → LUMO+1 HOMO-2 → LUMO HOMO-1 → LUMO+1 HOMO → LUMO	0.374 0.157 0.116 -0.147 0.542	MC
3	Triplet	1.6255	762.73	0.0000	HOMO-12 → LUMO+1 HOMO-8 → LUMO HOMO-7 → LUMO HOMO → LUMO+1	0.320 0.398 0.168 0.455	MC
4	Triplet	1.7983	689.46	0.0000	HOMO-12 → LUMO HOMO-11 → LUMO+1 HOMO-8 → LUMO+1 HOMO-1 → LUMO+1 HOMO → LUMO	0.120 0.344 -0.213 0.536 0.180	MC
5	Triplet	1.8275	678.44	0.0000	HOMO-12 → LUMO+1 HOMO-8 → LUMO HOMO-7 → LUMO HOMO-1 → LUMO HOMO → LUMO+1	-0.232 0.507 0.212 -0.149 -0.340	MC
6	Triplet	2.0416	607.29	0.0000	HOMO-11 → LUMO+1 HOMO-8 → LUMO+1 HOMO-7 → LUMO+1 HOMO-1 → LUMO+1	0.166 0.597 0.256 0.210	MC
7	Triplet	3.3767	367.17	0.0000	HOMO-23 → LUMO+1 HOMO-21 → LUMO HOMO-2 → LUMO HOMO-21 → LUMO	0.353 0.545 0.248 0.114	MC

8	Triplet	3.6352	341.06	0.0000	HOMO-14 → LUMO HOMO-4 → LUMO HOMO-3 → LUMO+1	0.208 0.637 -0.139	CT
9	Triplet	3.7213	333.17	0.0000	HOMO-23 → LUMO+1 HOMO-21 → LUMO HOMO-2 → LUMO	-0.201 -0.173 0.635	CT
10	Triplet	3.7437	331.18	0.0000	HOMO-17 → LUMO HOMO-5 → LUMO HOMO-4 → LUMO+1 HOMO-3 → LUMO	0.204 0.247 -0.289 0.533	CT
11	Triplet	3.8105	325.38	0.0000	HOMO-17 → LUMO HOMO-5 → LUMO HOMO-3 → LUMO	0.101 0.629 -0.281	CT
12	Triplet	3.8954	318.28	0.0000	HOMO-23 → LUMO HOMO-21 → LUMO+1 HOMO-11 → LUMO HOMO-2 → LUMO+1 HOMO-1 → LUMO HOMO → LUMO+1	0.155 0.157 0.163 0.604 -0.108 -0.154	CT

Table S15: Cartesian coordinates of optimized $[Co(PhB(MeIm)_3)_2]^{+1}$ metal complex geometry at the B3LYP/6-311G(d) /PCM(acetonitrile) calculation level for singlet, triplet and quintet states.*

Atom	**Singlet**			**Triplet**			**Quintet**		
Co	0.000001	0.000006	-0.000006	-0.000036	0.000018	0.000040	-0.000000	0.000005	0.000016
B	-3.163599	-0.221035	0.022501	-3.252232	0.180367	0.092606	-3.307574	-0.194734	-0.000015
N	-2.491524	-0.796568	1.325011	-2.692367	1.521084	-0.510633	-2.685031	-0.943946	1.244477
C	-1.138494	-0.722450	1.457050	-1.361231	1.636248	-0.767263	-1.345579	-0.908010	1.486614
N	-0.854948	-1.332252	2.646108	-1.183495	2.924287	-1.171911	-1.144681	-1.725766	2.556079
C	0.446551	-1.489929	3.288680	0.076762	3.502132	-1.624673	0.130834	-1.955728	3.226293
H	1.213273	-1.018948	2.682503	0.879364	2.797982	-1.416916	0.909546	-1.422373	2.686509
H	0.429811	-1.019568	4.274992	0.040483	3.699461	-2.699665	0.085426	-1.586672	4.254263
H	0.681704	-2.550605	3.407004	0.271087	4.440694	-1.099911	0.362101	-3.023592	3.243207
C	-2.018183	-1.820428	3.226703	-2.381814	3.622653	-1.136359	-2.336881	-2.303325	2.960342
H	-2.010320	-2.347869	4.168476	-2.457123	4.662282	-1.418380	-2.396293	-2.990279	3.791226
C	-3.036298	-1.494271	2.392295	-3.323597	2.742198	-0.705069	-3.296930	-1.822031	2.126021
H	-4.086607	-1.719539	2.469670	-4.372457	2.899586	-0.513467	-4.349160	-2.050584	2.090749

N	-2.603314	1.239249	-0.136713	-2.630285	-1.002882	-0.741574	-2.748463	1.286296	0.000015
C	-1.270638	1.489530	-0.162534	-1.295995	-1.230074	-0.841515	-1.426056	1.609169	0.000062
N	-1.154300	2.842196	-0.308770	-1.164289	-2.346309	-1.612950	-1.379358	2.969468	0.000114
C	0.066488	3.638886	-0.388067	0.067206	-3.013300	-2.024664	-0.170379	3.786236	0.000263
H	0.934376	2.989278	-0.344442	0.920132	-2.511649	-1.579604	0.697787	3.132439	0.000135
H	0.085177	4.199002	-1.326215	0.051637	-4.054845	-1.695461	-0.144950	4.422124	-0.888189
H	0.106852	4.346179	0.444181	0.160895	-2.989805	-3.113202	-0.144934	4.421793	0.888953
C	-2.414372	3.427569	-0.372965	-2.415678	-2.811145	-1.999317	-2.658415	3.501996	0.000053
H	-2.543891	4.493006	-0.488120	-2.534136	-3.688996	-2.616094	-2.843519	4.565777	0.000067
C	-3.316957	2.421681	-0.265173	-3.326998	-1.969377	-1.453229	-3.512365	2.444710	0.000007
H	-4.394414	2.448982	-0.269524	-4.402972	-1.981103	-1.507805	-4.589647	2.430877	-0.000033
N	-2.490421	-1.064261	-1.124063	-2.587520	0.087286	1.521730	-2.685014	-0.943909	-1.244521
C	-1.137243	-1.020400	-1.267648	-1.242316	-0.059147	1.650229	-1.345559	-0.907951	-1.486642
N	-0.852700	-1.872565	-2.296744	-0.996810	-0.051553	2.991036	-1.144638	-1.725704	-2.556106
C	0.448583	-2.163327	-2.891577	0.295031	-0.218980	3.651068	0.130899	-1.955689	-3.226270
H	1.216530	-1.578510	-2.396244	1.047045	-0.453208	2.902917	0.909577	-1.422235	-2.686536
H	0.680992	-3.226155	-2.786903	0.572891	0.695836	4.180533	0.362220	-3.023545	-3.243056
H	0.433194	-1.908196	-3.954141	0.234927	-1.039759	4.369650	0.085489	-1.586754	-4.254283
C	-2.015524	-2.474277	-2.759546	-2.175096	0.138298	3.694919	-2.336830	-2.303250	-2.960407
H	-2.006988	-3.192319	-3.565463	-2.200845	0.177087	4.773414	-2.396224	-2.990193	-3.791303
C	-3.034299	-1.975859	-2.016130	-3.165750	0.240077	2.770345	-3.296893	-1.821987	-2.126086
H	-4.084397	-2.213155	-2.043679	-4.219851	0.415147	2.908007	-4.349120	-2.050557	-2.090828
B	3.163603	0.221029	-0.022496	3.252227	-0.180438	-0.092472	3.307575	0.194740	0.000009
N	2.491541	0.796551	-1.325021	2.692436	-1.521157	0.510754	2.685020	0.943963	-1.244471
C	1.138509	0.722443	-1.457063	1.361329	-1.636298	0.767566	1.345567	0.908019	-1.486597
N	0.854974	1.332208	-2.646143	1.183583	-2.924419	1.171949	1.144659	1.725753	-2.556077
C	-0.446523	1.489902	-3.288716	-0.076625	-3.502261	1.624846	-0.130863	1.955707	-3.226282
H	-1.213266	1.019017	-2.682492	-0.879203	-2.797968	1.417470	-0.909533	1.422176	-2.686614
H	-0.681614	2.550582	-3.407125	-0.271175	-4.440655	1.099864	-0.362244	3.023550	-3.243020
H	-0.429822	1.019461	-4.274991	-0.040107	-3.699893	2.699774	-0.085385	1.586833	-4.254313
C	2.018216	1.820357	-3.226747	2.381853	-3.622853	1.136035	2.336852	2.303322	-2.960345
H	2.010361	2.347772	-4.168535	2.457161	-4.662545	1.417822	2.396256	2.990262	-3.791242
C	3.036323	1.494220	-2.392323	3.323620	-2.742350	0.704798	3.296908	1.822046	-2.126023
H	4.086630	1.719499	-2.469693	4.372435	-2.899795	0.512992	4.349138	2.050603	-2.090762

N	2.490416	1.064272	1.124050	2.587467	-0.087306	-1.521597	2.685029	0.943905	1.244528
C	1.137237	1.020429	1.267619	1.242257	0.059069	-1.650092	1.345575	0.907957	1.486659
N	0.852688	1.872635	2.296679	0.996750	0.051571	-2.990902	1.144670	1.725696	2.556135
C	-0.448609	2.163474	2.891442	-0.295100	0.218927	-3.650936	-0.130851	1.955653	3.226339
H	-1.216476	1.578230	2.396486	-1.047085	0.453386	-2.902832	-0.909573	1.422375	2.686494
H	-0.433077	1.908910	3.954138	-0.234952	1.039525	-4.369720	-0.085484	1.586513	4.254281
H	-0.681252	3.226197	2.786220	-0.573051	-0.695991	-4.180181	-0.362073	3.023526	3.243333
C	2.015511	2.474360	2.759468	2.175048	-0.138148	-3.694798	2.336866	2.303251	2.960415
H	2.006970	3.192434	3.565356	2.200801	-0.176794	-4.773299	2.396269	2.990200	3.791304
C	3.034289	1.975912	2.016077	3.165706	-0.239939	-2.770230	3.296923	1.821966	2.126100
H	4.084393	2.213186	2.043638	4.219829	-0.414887	-2.907884	4.349151	2.050526	2.090836
N	2.603309	-1.239251	0.136722	2.630288	1.002795	0.741734	2.748458	-1.286289	-0.000030
C	1.270632	-1.489525	0.162534	1.296005	1.230007	0.841685	1.426050	-1.609159	-0.000030
N	1.154286	-2.842202	0.308667	1.164326	2.346197	1.613202	1.379347	-2.969457	-0.000102
C	-0.066506	-3.638880	0.388028	-0.067151	3.013121	2.025080	0.170364	-3.786218	-0.000143
H	-0.934392	-2.989278	0.344262	-0.920137	2.511146	1.580500	-0.697799	-3.132416	-0.000225
H	-0.106825	-4.346292	-0.444120	-0.160455	2.990003	3.113659	0.144981	-4.421975	-0.888690
H	-0.085244	-4.198860	1.326257	-0.051899	4.054551	1.695496	0.144864	-4.421904	0.888453
C	2.414354	-3.427587	0.372814	2.415731	2.811052	1.999495	2.658402	-3.501990	-0.000122
H	2.543868	-4.493033	0.487899	2.534209	3.688863	2.616326	2.843502	-4.565771	-0.000176
C	3.316946	-2.421698	0.265082	3.327026	1.969272	1.453385	3.512356	-2.444706	-0.000068
H	4.394403	-2.449007	0.269421	4.403002	1.980964	1.507957	4.589637	-2.430878	-0.000071
C	-4.777554	-0.160550	0.016214	-4.862438	0.034471	0.075886	-4.925577	-0.111230	-0.000016
C	-5.514845	-0.169696	-1.184003	-5.536693	-0.814640	0.974995	-5.659515	0.023517	-1.194614
C	-5.512039	0.094971	1.190740	-5.646842	0.606094	-0.944294	-5.659512	0.023432	1.194595
C	-6.900475	0.001315	-1.208258	-6.912707	-1.037572	0.897814	-7.041875	0.220610	-1.201684
H	-5.003132	-0.282766	-2.135380	-4.979151	-1.340538	1.745401	-5.145675	0.003480	-2.151702
C	-6.897602	0.267598	1.180113	-7.023802	0.390431	-1.033060	-7.041871	0.220525	1.201683
H	-4.997788	0.193923	2.142331	-5.177774	1.217181	-1.710381	-5.145668	0.003323	2.151680
C	-7.602567	0.207760	-0.021416	-7.667004	-0.424944	-0.102632	-7.743914	0.307437	0.000004
H	-7.428996	-0.018019	-2.158736	-7.393315	-1.697618	1.616515	-7.567989	0.314750	-2.149062
H	-7.423881	0.458163	2.112765	-7.591698	0.855493	-1.835791	-7.567983	0.314597	2.149069
H	-8.681935	0.338436	-0.034699	-8.739401	-0.593369	-0.165483	-8.820780	0.458066	0.000011
C	4.777557	0.160533	-0.016149	4.862419	-0.034468	-0.075920	4.925578	0.111230	-0.000008

C	5.512132	-0.094932	-1.190629	5.647229	-0.606333	0.943776	5.659510	-0.023318	-1.194633
C	5.514755	0.169599	1.184128	5.536251	0.815099	-0.974954	5.659522	-0.023626	1.194576
C	6.897694	-0.267568	-1.179902	7.024188	-0.390470	1.032184	7.041868	-0.220415	-1.201745
H	4.997958	-0.193839	-2.142266	5.178506	-1.217781	1.709791	5.145663	-0.003115	-2.151715
C	6.900381	-0.001425	1.208484	6.912244	1.038246	-0.898118	7.041880	-0.220724	1.201622
H	5.002964	0.282619	2.135470	4.978367	1.341138	-1.745016	5.145686	-0.003674	2.151668
C	7.602565	-0.207805	0.021684	7.666956	0.425364	0.101867	7.743915	-0.307444	-0.000076
H	7.424044	-0.458086	-2.112524	7.592421	-0.855735	1.834558	7.567976	-0.314397	-2.149142
H	7.428827	0.017847	2.159005	7.392515	1.698632	-1.616732	7.567999	-0.314952	2.148989
H	8.681930	-0.338491	0.035045	8.739344	0.593942	0.164470	8.820780	-0.458075	-0.000101

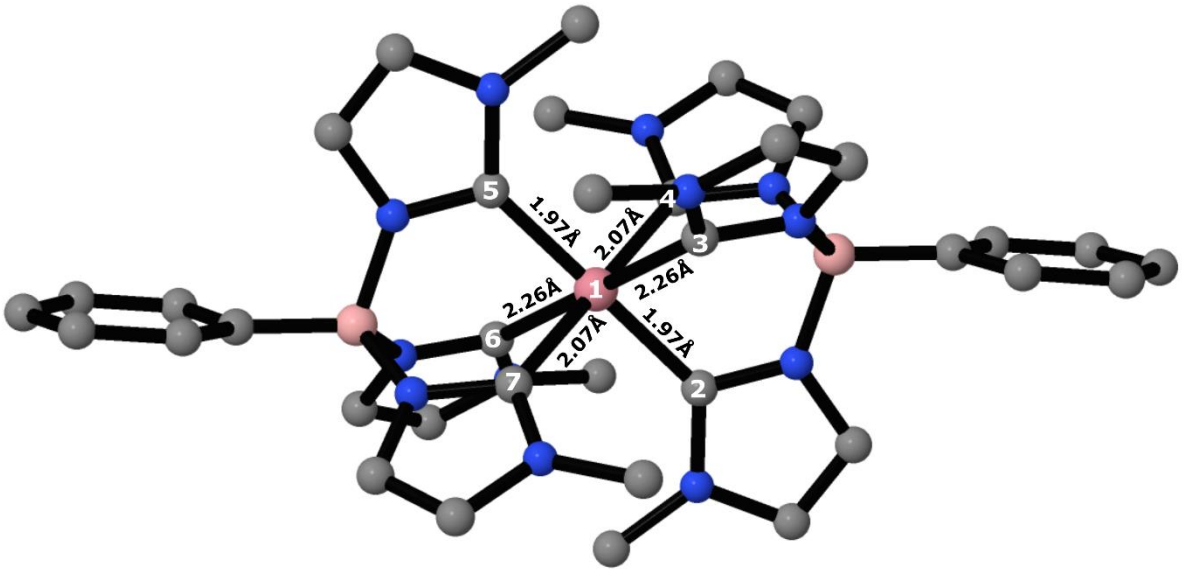

Figure S18: Optimzed ^{3}MC geometry including Co-C bond lenghths illustrating the symmetry distorted geonmetry around the Co centre. Calculations conducted at the B3LYP/6-311G(d) /PCM(acetonitrile) level of theory.*

References

(1) Forshaw, A. P.; Bontchev, R. P.; Smith, J. M. Oxidation of the Tris(Carbene)Borate Complex PhB(MeIm) 3 Mn I (CO) 3 to Mn IV [PhB(MeIm) 3] 2 (OTf) 2. *Inorg. Chem.* **2007**, *46* (10), 3792–3794. https://doi.org/10.1021/ic070187w.

(2) Kjær, K. S.; Kaul, N.; Prakash, O.; Chábera, P.; Rosemann, N. W.; Honarfar, A.; Gordivska, O.; Fredin, L. A.; Bergquist, K.; Häggström, L.; Ericsson, T.; Lindh, L.; Yartsev, A.; Styring, S.; Huang, P.; Uhlig, J.; Bendix, J.; Strand, D.; Sundström, V.; Persson, P.; Lomoth, R.; Wärnmark, K. Luminescence and Reactivity of a Charge-Transfer Excited Iron Complex with Nanosecond Lifetime. *Science (80-.).* **2019**, *363* (6424), 249–253. https://doi.org/10.1126/science.aau7160.

(3) Duchanois, T.; Etienne, T.; Cebrián, C.; Liu, L.; Monari, A.; Beley, M.; Assfeld, X.; Haacke, S.; Gros, P. C. An Iron-Based Photosensitizer with Extended Excited-State Lifetime: Photophysical and Photovoltaic Properties. *Eur. J. Inorg. Chem.* **2015**, *2015* (14), 2469–2477. https://doi.org/10.1002/ejic.201500142.

(4) Atkins, P.; De Paula, J. *Physical Chemistry*, 8th ed.; Oxford University Press: Oxford, 2006.

(5) Hammond, P. R. Laser Dye DCM, Its Spectral Properties, Synthesis and Comparison with Other Dyes in the Red. *Opt. Commun.* **1979**, *29* (3), 331–333. https://doi.org/10.1016/0030-4018(79)90111-1.

(6) Brackmann, U. *Lambdachrome® Laser Dyes*, 3rd ed.; Lambda Physik AG: Göttingen, 2000.

(7) Sharpe, A. G.; Housecroft, C. E. *Inorganic Chemistry*, 4th ed.; Pearson: Harlow, England, 2012.

(8) Technologies, A. CrysAlis PRO. Agilent Technologies 2011.

(9) Farrugia, L. J. WinGX and ORTEP for Windows : An Update. *J. Appl. Crystallogr.* **2012**, *45* (4), 849–854. https://doi.org/10.1107/S0021889812029111.

(10) Palatinus, L.; Chapuis, G. SUPERFLIP – a Computer Program for the Solution of Crystal Structures by Charge Flipping in Arbitrary Dimensions. *J. Appl. Crystallogr.* **2007**, *40* (4), 786–790. https://doi.org/10.1107/S0021889807029238.

(11) Sheldrick, G. M. A Short History of SHELX. *Acta Crystallogr. Sect. A Found. Crystallogr.* **2008**, *64* (1), 112–122. https://doi.org/10.1107/S0108767307043930.

(12) Becke, A. D. Density-functional Thermochemistry. III. The Role of Exact Exchange. *J. Chem. Phys.* **1993**, *98* (7), 5648–5652. https://doi.org/10.1063/1.464913.

(13) Reiher, M.; Salomon, O.; Artur Hess, B. Reparameterization of Hybrid Functionals Based on Energy Differences of States of Different Multiplicity. *Theor. Chem. Accounts Theory, Comput. Model. (Theoretica Chim. Acta)* **2001**, *107* (1), 48–55. https://doi.org/10.1007/s00214-001-0300-3.

(14) Krishnan, R.; Binkley, J. S.; Seeger, R.; Pople, J. A. Self-consistent Molecular Orbital Methods. XX. A Basis Set for Correlated Wave Functions. *J. Chem. Phys.* **1980**, *72* (1), 650–654. https://doi.org/10.1063/1.438955.

(15) McLean, A. D.; Chandler, G. S. Contracted Gaussian Basis Sets for Molecular Calculations. I. Second Row Atoms, Z =11–18. *J. Chem. Phys.* **1980**, *72* (10), 5639–5648. https://doi.org/10.1063/1.438980.

(16) Frisch, M. J.; Trucks, G. W.; Schlegel, H. B.; Scuseria, G. E.; Robb, M. A.; Cheeseman, J. R.; Scalmani, G.; Barone, V.; Mennucci, B.; Petersson, G. A.; Nakatsuji, H.; Caricato, M.; Li, X.; Hratchian, H. P.; Izmaylov, A. F.; Bloino, J.; Zheng, G.; Sonnenberg, J. L.; Hada, M.; Ehara, M.;

Toyota, K.; Fukuda, R.; Hasegawa, J.; Ishida, M.; Nakajima, T.; Honda, Y.; Kitao, O.; Nakai, H.; Vreven, T.; Montgomery, J. A. J.; Peralta, J. E.; Ogliaro, F.; Bearpark, M.; Heyd, J. J.; Brothers, E.; Kudin, K. N.; Staroverov, V. N.; Keith, T.; Kobayashi, R.; Normand, J.; Raghavachari, K.; Rendell, A.; Burant, J. C.; Iyengar, S. S.; Tomasi, J.; Cossi, M.; Rega, N.; Millam, J. M.; Klene, M.; Knox, J. E.; Cross, J. B.; Bakken, V.; Adamo, C.; Jaramillo, J.; Gomperts, R.; Stratmann, R. E.; Yazyev, O.; Austin, A. J.; Cammi, R.; Pomelli, C.; Ochterski, J. W.; Martin, R. L.; Morokuma, K.; Zakrzewski, V. G.; Voth, G. A.; Salvador, P.; Dannenberg, J. J.; Dapprich, S.; Daniels, A. D.; Farkas, O.; Foresman, J. B.; Ortiz, J. V.; Cioslowski, J.; Fox, D. J. Gaussian 09, Revision E.01. Gaussian, Inc.: Wallingford CT 2013.